ЖЭТФ, 2003, том 124, вып. 2 (8), стр. 445–476

X-RAY OPTICAL ACTIVITY: APPLICATIONS OF SUM RULES

J. Goulon, A. Rogalev*, F. Wilhelm, C. Goulon-Ginet, P. Carra, I. Marri

European Synchrotron Radiation Facility
38043, Grenoble Cedex, France

Ch. Brouder

Laboratoire de Minéralogie-Cristallographie UMR-CNRS 7590, Université Paris-VI, IPGP
F-75252, Paris, Cedex 05, France

Submitted 20 December 2002

Edge-selective sum rules are proposed for a variety of X-ray dichroisms related to natural or nonreciprocal optical activity. Four spherical operators are identified that mix orbitals of different parities in what is assumed to be the ground state. The orbital anapole moment $\mathbf{\Omega}^{(1)}$ is primarily responsible for the magnetochiral dichroism; the time-even rank-2 tensor $\mathbf{N}^{(2)} = [\mathbf{L}, \mathbf{\Omega}]^{(2)}$ for natural circular dichroism; the time-odd rank-2 tensor $\mathbf{W}^{(2)} = [\mathbf{L}, \mathbf{n}]^{(2)}$ for nonreciprocal magnetic linear dichroisms. At higher orders, the time-odd rank-3 tensor $\mathbf{\Gamma}^{(3)} = [\mathbf{L}, \mathbf{L}, \mathbf{\Omega}]^{(3)}$ can also contribute to all nonreciprocal dichroisms. The physical content of these operators is analyzed. For every magnetoelectric group, one can predict which dichroic effect can be measured with either a single crystal or a powdered sample. Experimental spectra are produced to illustrate the value of the sum rules and the practical conditions of their application. Regarding nonreciprocal activity, one should be cautious about discussing magnetic symmetry because the deep core hole can couple the true ground state with low-lying excited states.

PACS: 78.70.Dm, 78.20.Ls, 75.80.+q

CONTENTS

1. Introduction 446

2. Edge-selective $E1E2$ sum rules 447
2.1. Parity-mixing operators 447
2.2. Spherical polarization tensors 447
2.3. Symmetry groups in XOA 448
2.3.1. Transformation properties 448
2.3.2. Symmetry groups and $E1E2$ absorption . 450
2.4. Effective operators of XOA 450
2.4.1 Spherical basis 450
2.4.2. Cartesian basis 451

3. Physical implications 453
3.1. Orbital magnetoelectric operators 453
3.1.1. Spin and orbital anapoles 453
3.1.2. Operators conserved by $I\Theta$ 453
3.1.3. Operators not conserved by $I\Theta$ 456
3.2. Natural X-ray optical activity 457
3.3. Rotational isotropy 458
3.3.1. XNCD spectra 458
3.3.2. Nonreciprocal XMχD and XMLD spectra 459

4. Applications of X-ray optical activity . 463
4.1. Magnetoelectric symmetry 463
4.1.1. Chromium sesquioxide: Cr_2O_3 463
4.1.2. Vanadium sesquioxides: $(V_{1-x}Cr_x)_2O_3$ .. 466
4.2. Effective operators and cross densities of states 469
4.2.1. Applications of the XOA sum rules 469
4.2.2. Cross densities of states 471

5. Conclusion 472

Appendix 473

References 473

*E-mail: rogalev@esrf.fr

1. INTRODUCTION

Systems with broken inversion symmetry play a fascinating role not only in physics but also in chemistry and in life sciences where molecular recognition processes are very often controlled by chirality. In 1958, Zel'dovich [1] introduced the concept of the anapole to describe parity-violating interactions. For nearly 40 years, atomic and nuclear physicists were angling for nuclear anapoles [2, 3] until the anapole moment of ^{133}Cs was finally measured in 1997 [4]. In solid-state physics, the concept of the anapole has attracted much less attention even though there is a long established literature dealing with toroidal multipole moments [5–8]. It was realized recently that X-ray optical activity (XOA) can offer a unique experimental access to orbital anapole moments and to a whole family of related operators. It is the aim of the present paper to analyze the physical content of these operators, especially for magnetoelectric solids in which parity (I) and time-reversal (Θ) symmetries are broken, while the structure remains invariant under the product $I\Theta$ [9].

Unlike magneto-optical effects such as the Faraday rotation or the magnetic circular dichroism, which refer primarily to electric dipole ($E1E1$) transitions, optical activity is associated with transition probabilities that mix multipole moments of opposite parities (e.g., $E1M1$ or $E1E2$). The Curie principle thus states that optical activity can be observed only in parity nonconserving systems. We recall that properties related to optical activity can be either even («natural») or odd («nonreciprocal») with respect to the time-reversal operator Θ. We have discussed elsewhere [10] how to transpose the theories of optical activity currently used at optical wavelengths into the X-ray spectral range. Following Buckingham [11] and Barron [12], we found it most convenient to describe XOA by introducing a complex gyration tensor

$$\zeta_{\alpha\beta\gamma} = \zeta'_{\alpha\beta\gamma} - i\zeta''_{\alpha\beta\gamma}.$$

In core level spectroscopies, magnetic dipole transitions ($M1$) are very weak [13], and it seems perfectly legitimate to neglect the $E1M1$ terms. Under such conditions, this Cartesian gyration tensor is dominated by the electric dipole ($E1_\alpha$)–electric quadrupole ($E2_{\beta\gamma}$) interference terms,

$$\begin{aligned} \zeta'_{\alpha\beta\gamma} &= \mathrm{Im}\left\{E1_\alpha E2_{\beta\gamma}\right\} + \mathrm{Im}\left\{E1_\beta E2_{\alpha\gamma}\right\}, \\ \zeta''_{\alpha\beta\gamma} &= \mathrm{Re}\left\{E1_\alpha E2_{\beta\gamma}\right\} - \mathrm{Re}\left\{E1_\beta E2_{\alpha\gamma}\right\}. \end{aligned} \qquad (1)$$

The imaginary part (ζ'') is antisymmetric with respect to interchange of the α, β subscripts and is responsible for the natural XOA; the real part (ζ') is symmetric and contributes to nonreciprocal effects [12].

Every Stokes component S_j is associated with a well identified dichroism related to XOA [14–19]:

1)The X-ray magnetochiral dichroism (XMχD),

$$\mathrm{XM}\chi\mathrm{D}(S_0) \propto \left[\zeta'_{\beta\beta\gamma} + \zeta'_{\alpha\alpha\gamma}\right].$$

2) The nonreciprocal X-ray magnetic linear dichroism (XMLD),

$$\mathrm{XMLD}(S_1) \propto \left[\zeta'_{\beta\beta\gamma} - \zeta'_{\alpha\alpha\gamma}\right].$$

3) The nonreciprocal, Jones X-ray magnetic linear dichroism (XMLD),

$$\mathrm{XMLD}(S_2) \propto 2\zeta'_{\alpha\beta\gamma}.$$

4) The X-ray natural circular dichroism (XNCD),

$$\mathrm{XNCD}(S_3) \propto 2\zeta''_{\alpha\beta\gamma}.$$

In several cases, XNCD spectra were successfully reproduced using *ab initio* calculations in the general framework of the multiple scattered wave theory [16, 20]. To the best of our knowledge, however, no suitable code for simulation of the nonreciprocal XOA is presently available. This is why we focus in this paper on the exploitation of edge-selective sum rules, which may give access to the expectation values of a series of effective operators that mix orbitals of opposite parities in what is assumed to be the true multi-electronic ground state $|\psi_g\rangle$. In the next section, we recast the XOA sum rules in their general framework. In Sec. 3, we analyze the physical content of the four effective operators that were identified as responsible for XOA. An important result in this section is the possibility to predict which dichroism can be observed experimentally for a given magnetic class. In Sec. 4, referring to several specific examples, we develop some considerations on what can be learnt regarding the magnetoelectric symmetry and how the XOA operators can be accessed in practice.

Throughout this paper, we keep the same terminology (i.e., scalar, vector, deviator, septor, ...) for the decomposition of Cartesian or spherical tensors into their irreducible representations [21, 22]. We systematically use normal fonts for Cartesian tensors and bold face fonts for spherical tensors. Irreducible tensors of an even rank that have odd parity or irreducible tensors of an odd rank with even parity are commonly called pseudotensors. For clarity, we prefer to call irreducible tensors of an odd rank and odd parity polar tensors rather than true tensors. Polar vectors that are odd under time reversal are called toroidal for reasons explained in Sec. 3; pseudovectors that are even under time reversal are called antitoroidal by analogy.

2. EDGE-SELECTIVE $E1E2$ SUM RULES

2.1. Parity-mixing operators

Optical sum rules are commonly used in atomic physics [23]. In 1992, Thole et al. [24] established a useful sum rule for X-ray magnetic circular dichroism (XMCD): it states that the integrated dichroic signal is proportional to $\langle L_z \rangle$, i.e., to the ground state expectation value of the angular momentum operator acting on the electronic shell that accepts the excited photelectron. For XMCD spectra, one is mostly concerned with electric dipole ($E1$) transitions satisfying the selection rule $\ell = \ell_c \pm 1$, where ℓ_c characterizes the angular momentum in the initial core state and ℓ is the angular momentum in the final excited state. In 1998, using a similar approach, Natoli et al. [20] already established the sum rule

$$\Sigma_{E1E2} = \int\limits_{\Delta E} \frac{\sigma_{E1E2}(E)}{E^2} dE \propto \langle \psi_g | \mathbf{N}^{(2)}(\ell, \ell') | \psi_g \rangle \quad (2)$$

for X-ray natural circular dichroism (XNCD), where σ_{E1E2} denotes the X-ray absorption cross section due to the $E1E2$ interference terms in a finite energy range ΔE that must include, whenever this is relevant, the two partners (j_+, j_-) of the spin–orbit split edge. In the right-hand side, ℓ still refers to the final angular momentum of the electric dipole ($E1$) transition and ℓ' refers to the electric quadrupole transition ($E2$) satisfying the selection rule $\ell' = \ell_c \pm 0, 2$, excluding $\ell' = \ell_c = 0$. Obviously, ℓ and ℓ' have opposite parities and the operator $\mathbf{N}^{(2)}(\ell, \ell')$ probes the mixing of atomic orbitals of the corresponding parities. The problem with Eq. (2) was that the rank-2 spherical tensor $\mathbf{N}^{(2)}$ was given no clear physical meaning in Ref. [20]. We also found it desirable to extend this sum rule to all $E1E2$ dichroisms.

Regarding Eq. (2), there is still a serious limitation that was underlined by Di Matteo and Natoli in a comprehensive review article [25]. Due to the core hole perturbation, $|\psi_g\rangle$ is merely a virtual or pseudo ground state of the system. Intuitively, one may fear that the core hole does affect orbitals of opposite parities differently. If we expand $|\psi_g\rangle$ in terms of stationary states $|\Psi_n\rangle$, the quantity that is obtained is actually given by

$$\langle \psi_g | \mathbf{O}^{(q)} | \psi_g \rangle = \sum_{n,n'} \alpha_n^* \alpha_{n'} \langle \Psi_n | \mathbf{O}^{(q)} | \Psi_{n'} \rangle, \quad (3)$$

where $\mathbf{O}^{(q)}$ is the pertinent parity-mixing effective operator. At present, there is no proof that the sum over all configurations cancels the effects of the core hole and restores the property of a true ground state as this is implicitly assumed for the popular XMCD sum rules. Contrary to Ref. [25], we are not even certain that the cross terms ($n \neq n'$) can *a priori* be neglected: typically, in the case of XMCD where $\mathbf{O}^{(1)} = L_z$, the matrix elements in the right-hand side of Eq. (3) are precisely those that contribute to the Van Vleck paramagnetism and are usually nonzero. We consider this difficulty again in Sec. 4.

2.2. Spherical polarization tensors

The electric dipole ($E1$) and electric quadrupole ($E2$) transition operators are $\hat{\epsilon} \cdot \mathbf{r}$ and $\hat{\epsilon} \cdot \mathbf{r}\,\mathbf{k} \cdot \mathbf{r}$, respectively. We recall that for the left circularly polarized light with a wavevector $\mathbf{k}$, $\hat{\epsilon} = (\mathbf{i} - i\mathbf{j})/\sqrt{2}$ where $\mathbf{i}$ and $\mathbf{j}$ are unit vectors such that

$$\mathbf{i} \times \mathbf{j} = \mathbf{k}/k = \hat{k}.$$

It is therefore natural to describe the angular dependence of the interference between the $E1$ and $E2$ transitions by coupling $\hat{\epsilon}$ first with $\hat{k}$ (as spherical tensors) and then with $\hat{\epsilon}^*$ to obtain

$$\mathbf{T}_\beta^{(b)} = [\hat{\epsilon}^*, [\hat{\epsilon}, \hat{k}]^{(2)}]_\beta^{(b)}$$

([,] denotes a coupling via Clebsch–Gordan coefficients). The coupling of spherical tensors is described in standard textbooks (e.g., [26]). But the tensors $\mathbf{T}_\beta^{(b)}$ do not have a well-defined behavior under time reversal and are to be decomposed into their time-reversal even ($\theta = 1$) and time-reversal odd ($\theta = -1$) parts $\mathbf{T}_\beta^{(b,\theta)}$. The $E1E2$ absorption cross section (σ_{E1E2}) and sum rules (Σ_{E1E2}) are therefore written as

$$\sigma_{E1E2} = \sum_{b=1}^{3} \sum_{\beta=-b}^{b} \sum_{\theta=\pm 1} (-1)^\beta \mathbf{T}_\beta^{(b,\theta)} \boldsymbol{\sigma}_{-\beta}^{(b,\theta)},$$

$$\Sigma_{E1E2} = \sum_{b=1}^{3} \sum_{\beta=-b}^{b} \sum_{\theta=\pm 1} (-1)^\beta \mathbf{T}_\beta^{(b,\theta)} \boldsymbol{\Sigma}_{-\beta}^{(b,\theta)},$$

where $\boldsymbol{\sigma}_{-\beta}^{(b,\theta)}$ and $\boldsymbol{\Sigma}_{-\beta}^{(b,\theta)}$ are rank-b spherical tensors.

To investigate the time-reversal symmetry of $\mathbf{T}_\beta^{(b,\theta)}$, we write it in terms of

$$\mathbf{X}_\beta^{(a,b)} = [[\hat{\epsilon}^*, \hat{\epsilon}]^{(a)}, \hat{k}]_\beta^{(b)}$$

(see [27] and Table 1). Here, $[\hat{\epsilon}^* \otimes \hat{\epsilon}]^{(a)}$ is a rank-a spherical tensor. As proved in the next section, the time reversal properties of $\mathbf{X}_\beta^{(a,b)}$ can readily be deduced from the fact that the action of the time-reversal operator Θ on $\hat{\epsilon}$ and $\mathbf{k}$ is $\Theta\hat{\epsilon} = \hat{\epsilon}^*$ and $\Theta\mathbf{k} = -\mathbf{k}$. The action of Θ on $\mathbf{X}_\beta^{(a,b)}$ is therefore given by

$$\Theta \mathbf{X}_\beta^{(a,b)} = (-1)^{a+1} \mathbf{X}_\beta^{(a,b)}.$$

Table 1. Polarization tensors of XOA

$\mathbf{T}^{(1,+1)} \equiv 0$ (transversality condition)		
$a=0$	$\mathbf{T}_0^{(1,-1)}(\hat{k}) = -\frac{1}{2}\sqrt{\frac{3}{5}}\,\hat{k}$	XMχD (S_0)
$a=2$	$\mathbf{T}_0^{(2,+1)}(\hat{\epsilon},\hat{k}) = \frac{\sqrt{3}}{2}\left[[\hat{\epsilon}^*,\hat{\epsilon}]^{(1)},\hat{k}\right]_0^{(2)}$	XNCD (S_3)
$a=2$	$\mathbf{T}_{\pm 2}^{(2,-1)}(\hat{\epsilon},\hat{k}) = \frac{1}{2}\left[[\hat{\epsilon}^*,\hat{\epsilon}]^{(2)},\hat{k}\right]_{\pm 2}^{(2)}$	XMLD (S_1,S_2)
$\mathbf{T}^{(3,+1)} \equiv 0$		
$a=2$	$\mathbf{T}_0^{(3,-1)}(\hat{\epsilon},\hat{k}) = \left[[\hat{\epsilon}^*,\hat{\epsilon}]^{(2)},\hat{k}\right]_0^{(3)}$	XMχD (S_0)
$a=2$	$\mathbf{T}_{\pm 2}^{(3,-1)}(\hat{\epsilon},\hat{k}) = \left[[\hat{\epsilon}^*,\hat{\epsilon}]^{(2)},\hat{k}\right]_{\pm 2}^{(3)}$	XMLD (S_1,S_2)

We note that complex conjugation has a different action,

$$\mathbf{X}_\beta^{(a,b)\,*} = (-1)^{a+1+b-\beta}\mathbf{X}_{-\beta}^{(a,b)}.$$

We now consider the possible values of a and b satisfying the triangle conditions $0 \le a \le 2$ and $|a-1| \le b \le a+1$.

1) For $a=0$, i.e., $\hat{\epsilon}^* \cdot \hat{\epsilon} = 1$, it immediately follows that $b=1$ and $\sigma_{E1E2} \propto \hat{k}\sigma^{(1,-1)}$ or $\Sigma_{E1E2} \propto \hat{k}\Sigma^{(1,-1)}$. This is obviously the case of XMχD.

2) For $a=1$, i.e., $[\hat{\epsilon}^*,\hat{\epsilon}]^{(1)} \propto i\hat{k}$, the result is still rather simple if we assume that the electromagnetic wave remains transverse inside the sample, i.e., if the condition $\widehat{\epsilon} \cdot \mathbf{k} = 0$ is satisfied; then, the only choice for b is 2. This is typically the case of XNCD and it was previously established that the spherical tensors $\boldsymbol{\sigma}^{(2,+1)}$and $\boldsymbol{\Sigma}^{(2,+1)}$ are rank-2 pseudodeviators [20].

3) Finally, if $a=2$, the problem becomes more complicated because the values $b=1,2,3$ are possible, which implies that the tensor property $\sigma^{(b,-1)}$ can be a vector, a deviator or a septor. The option $\{a=2; b=1\}$ again yields the same vector contribution to XMχD; the options $\{a=2; b=2,3\}$ can be shown to contribute to nonreciprocal XMLD.

This discussion and the relation between $\mathbf{T}_\beta^{(b,\theta)}$ and $\mathbf{X}_\beta^{(a,b)}$ show that the nonzero tensors are $\mathbf{T}^{(1,-1)}$, $\mathbf{T}^{(2,+1)}$, $\mathbf{T}^{(2,-1)}$, and $\mathbf{T}^{(3,-1)}$. These tensors transform as

$$\Theta\mathbf{T}_\beta^{(b,\theta)} = \theta\mathbf{T}_\beta^{(b,\theta)}$$

under time-reversal symmetry and as

$$\mathbf{T}_\beta^{(b,\theta)\,*} = \theta(-1)^{b-\beta}\mathbf{T}_{-\beta}^{(b,\theta)}$$

under complex conjugation. We note that all tensors $\boldsymbol{\sigma}^{(b,\theta)}$ and $\boldsymbol{\Sigma}^{(b,\theta)}$ are time-reversal odd with the unique exception of XNCD $\{a=1;\ b=2\}$.

At this stage, within the limits of validity of Eqs. (2), several important results already follow without heavy calculations: because the effective vector operator of XMχD is odd under I and Θ, it can only be a toroidal vector; the effective operator of XNCD must be a time-even pseudodeviator; the effective operators of XMLD (S_1, S_2) must combine a pseudodeviator and a polar septor, which must again be odd with respect to both I and Θ. These results are summarized in Table 1.

2.3. Symmetry groups in XOA

In magnetic samples, the time-reversal operator Θ plays a key role and the point and space groups have to be replaced by magnetic point and space groups [29]. The representation theory of magnetic groups is difficult because Θ is antilinear and representations are replaced by corepresentations [30]. Theorems involving characters are no longer valid for corepresentations because the equivalence between corepresentations D and D' is not determined by the existence of a matrix A such that $D' = ADA^{-1}$ [30]. Nevertheless, we show that these complications can be circumvented for the representations of symmetries involved in XOA.

2.3.1. Transformation properties

The X-ray absorption cross section σ including electric dipole and quadrupole transitions is proportional to

$$\sigma(\hat{\epsilon},\mathbf{k}) \propto \sum_f \langle\psi_g|\hat{\epsilon}^* \cdot \mathbf{r} - \frac{i}{2}\hat{\epsilon}^* \cdot \mathbf{r}\,\mathbf{k} \cdot \mathbf{r}|\psi_f\rangle \times$$
$$\times \langle\psi_f|\hat{\epsilon} \cdot \mathbf{r} + \frac{i}{2}\hat{\epsilon} \cdot \mathbf{r}\,\mathbf{k} \cdot \mathbf{r}|\psi_g\rangle\delta(E_f - E_g - \hbar\omega).$$

We now successively transform a physical state with the parity I, time-reversal Θ, rotation R, and translation $T_{\mathbf{R}}$ operations and consider how $\sigma(\hat{\epsilon}, \mathbf{k})$ is modified.

To investigate the transformation of the absorption cross section under parity, we first consider the one-electron spinless case. The action of the parity operator (I) on the system transforms the wavefunctions as $(I\psi_f)(\mathbf{r}) = \psi_f(-\mathbf{r})$ and $(I\psi_g)(\mathbf{r}) = \psi_g(-\mathbf{r})$, and the matrix elements become

$$\langle I\psi_f|\hat{\epsilon}\cdot\mathbf{r}|I\psi_g\rangle = \int \mathrm{d}\mathbf{r}\psi_f^*(-\mathbf{r})\hat{\epsilon}\cdot\mathbf{r}\psi_g(-\mathbf{r}) =$$
$$= \int \mathrm{d}\mathbf{r}'\psi_f^*(\mathbf{r}')\ \hat{\epsilon}\cdot(-\mathbf{r}')\psi_g(\mathbf{r}') = \langle\psi_f|(-\hat{\epsilon})\cdot\mathbf{r}|\psi_g\rangle.$$

The same result holds generally for a many-body system with spin. Moreover,

$$\langle I\psi_f|\hat{\epsilon}\cdot\mathbf{r} + \frac{i}{2}\hat{\epsilon}\cdot\mathbf{r}\,\mathbf{k}\cdot\mathbf{r}|I\psi_g\rangle =$$
$$= \langle\psi_f|I(\hat{\epsilon}\cdot\mathbf{r} + \frac{i}{2}\hat{\epsilon}\cdot\mathbf{r}\,\mathbf{k}\cdot\mathbf{r})I|\psi_g\rangle =$$
$$= \langle\psi_f|(-\hat{\epsilon})\cdot\mathbf{r} + \frac{i}{2}(-\hat{\epsilon})\cdot\mathbf{r}\,(-\mathbf{k})\cdot\mathbf{r}|\psi_g\rangle.$$

Therefore, if $\sigma(\hat{\epsilon}, \mathbf{k}; I)$ denotes the absorption cross section of the system transformed by parity, and if parity is a symmetry of the system (such that the energies of $I\psi_f$ and $I\psi_g$ coincide with the respective energies of ψ_f and ψ_g), we obtain that $\sigma(\hat{\epsilon}, \mathbf{k}; I) = \sigma(-\hat{\epsilon}, -\mathbf{k})$.

For time-reversal symmetry (Θ), we start from the basic equation

$$\langle\Theta\phi|\Theta\psi\rangle = \langle\phi|\psi\rangle^* = \langle\psi|\phi\rangle$$

(see [30, 31]). Hence,

$$\langle\Theta\psi_g|\Theta(\hat{\epsilon}\cdot\mathbf{r} + \frac{i}{2}\hat{\epsilon}\cdot\mathbf{r}\,\mathbf{k}\cdot\mathbf{r})|\psi_f\rangle =$$
$$= \langle\psi_g|\hat{\epsilon}\cdot\mathbf{r} + \frac{i}{2}\hat{\epsilon}\cdot\mathbf{r}\,\mathbf{k}\cdot\mathbf{r}|\psi_f\rangle^* = \langle\psi_f|\hat{\epsilon}^*\cdot\mathbf{r} - \frac{i}{2}\hat{\epsilon}^*\cdot\mathbf{r}\,\mathbf{k}\cdot\mathbf{r}|\psi_g\rangle.$$

On the other hand, the antilinearity of the time-reversal operator yields

$$\left|\Theta\left(\hat{\epsilon}\cdot\mathbf{r} + \frac{i}{2}\hat{\epsilon}\cdot\mathbf{r}\,\mathbf{k}\cdot\mathbf{r}\right)\psi_f\right\rangle =$$
$$= \left(\hat{\epsilon}^*\cdot\mathbf{r} - \frac{i}{2}\hat{\epsilon}^*\cdot\mathbf{r}\,\mathbf{k}\cdot\mathbf{r}\right)|\Theta\psi_f\rangle,$$

and therefore,

$$\langle\Theta\psi_g|\hat{\epsilon}^*\cdot\mathbf{r} - \frac{i}{2}\hat{\epsilon}^*\cdot\mathbf{r}\,\mathbf{k}\cdot\mathbf{r}|\Theta\psi_f\rangle =$$
$$= \langle\psi_f|\hat{\epsilon}^*\cdot\mathbf{r} - \frac{i}{2}\hat{\epsilon}^*\cdot\mathbf{r}\,\mathbf{k}\cdot\mathbf{r}|\psi_g\rangle.$$

Similarly,

$$\langle\Theta\psi_f|\hat{\epsilon}\cdot\mathbf{r} + \frac{i}{2}\hat{\epsilon}\cdot\mathbf{r}\,\mathbf{k}\cdot\mathbf{r}|\Theta\psi_g\rangle =$$
$$= \langle\psi_g|\hat{\epsilon}\cdot\mathbf{r} + \frac{i}{2}\hat{\epsilon}\cdot\mathbf{r}\,\mathbf{k}\cdot\mathbf{r}|\psi_f\rangle.$$

Finally, if $\sigma(\hat{\epsilon}, \mathbf{k}; \Theta)$ denotes the absorption cross section of the time-reversed system and if the system is invariant under Θ, we obtain that $\sigma(\hat{\epsilon}, \mathbf{k}; \Theta) = \sigma(\hat{\epsilon}^*, -\mathbf{k})$.

We next consider a transformation by the rotation R. Starting again with the one-electron spinless case, we have

$$\langle R\psi_f|\hat{\epsilon}\cdot\mathbf{r}|R\psi_g\rangle = \int \mathrm{d}\mathbf{r}\,\psi_f^*(R\mathbf{r})\,\hat{\epsilon}\cdot\mathbf{r}\,\psi_g(R\mathbf{r}) =$$
$$= \int \mathrm{d}\mathbf{r}'\psi_f^*(\mathbf{r}')\,\hat{\epsilon}\cdot(R^{-1}\mathbf{r}')\,\psi_g(\mathbf{r}') = \langle\psi_f|(R\hat{\epsilon})\cdot\mathbf{r}|\psi_g\rangle.$$

More generally, for a many-body system with spin, if $\sigma(\hat{\epsilon}, \mathbf{k}; R)$ denotes the absorption cross section of the system transformed by the rotation R, we find that

$$\sigma(\hat{\epsilon}, \mathbf{k}; R) = \sigma(R\hat{\epsilon}, R\mathbf{k}).$$

The last tranformation that we need is translation. In X-ray absorption spectroscopy, the dipole and quadrupole approximations are valid because the core states are localized and the origin of coordinates can be taken at the absorbing atom. If the system is translated, the origin is no longer the absorbing atom, the dipole and quadrupole approximations are not valid, and we must use the full absorption cross section [32]

$$\sigma(\hat{\epsilon}, \mathbf{k}) = \frac{4\pi^2\hbar\alpha}{m^2\omega}\sum_f |\langle\psi_f|e^{i\mathbf{k}\cdot\mathbf{r}}X|\psi_g\rangle|^2\delta(E_f - E_g - \hbar\omega),$$

where

$$X = \hbar\hat{\epsilon}\cdot\nabla - (g/2)\mathbf{s}\cdot(\mathbf{k}\times\hat{\epsilon})$$

and $\mathbf{s}$ is the spin operator. The operator X is not modified by translation. Thus, the translation $T_{\mathbf{R}}$ acting on the system by $T_{\mathbf{R}}\psi_f(\mathbf{r}) = \psi_f(\mathbf{r}+\mathbf{R})$ and $T_{\mathbf{R}}\psi_g(\mathbf{r}) = \psi_g(\mathbf{r}+\mathbf{R})$ transforms $\langle\psi_f|e^{i\mathbf{k}\cdot\mathbf{r}}X|\psi_g\rangle$ into

$$\langle T_{\mathbf{R}}\psi_f|e^{i\mathbf{k}\cdot\mathbf{r}}X|T_{\mathbf{R}}\psi_g\rangle = e^{-i\mathbf{k}\cdot\mathbf{R}}\langle\psi_f|e^{i\mathbf{k}\cdot\mathbf{r}}X|\psi_g\rangle.$$

Therefore, if $T_{\mathbf{R}}$ is a symmetry of the system, we obtain that $\sigma(\hat{\epsilon}, \mathbf{k}; T_{\mathbf{R}}) = \sigma(\hat{\epsilon}, \mathbf{k})$ and the absorption cross section is independent of translations of the system.

At this stage, we have shown that a transformation of the physical system can be replaced by a simultaneous transformation of the polarization and wave vectors. We next analyze the consequences of this result for the angular and polarization dependence of σ_{E1E2}.

2.3.2. Symmetry groups and $E1E2$ absorption

As discussed in Sec. 2.2, the $E1E2$ absorption cross section can be written as

$$\sigma_{E1E2} = \sum_{b=1}^{3} \sum_{\beta=-b}^{b} (-1)^{\beta} \sum_{\theta=\pm 1} \mathbf{T}_{\beta}^{(b,\theta)}\, \sigma_{-\beta}^{(b,\theta)}. \qquad (4)$$

In a reference frame where the wave vector is directed along z axis, the polarization vector is

$$\hat{\epsilon} = \begin{pmatrix} \cos\psi\cos\chi + i\sin\psi\sin\chi \\ \sin\psi\cos\chi - i\cos\psi\sin\chi \\ 0 \end{pmatrix},$$

which represents an elliptically polarized wave for which the ellipse axes are at the angle ψ with the reference frame axes, and the circular polarization rate is $\sin 2\chi$. We recall that

$$S_1/S_0 = \cos 2\chi \cos 2\psi, \quad S_2/S_0 = \cos 2\chi \sin 2\psi,$$

$$S_3/S_0 = \sin 2\chi.$$

In this frame, the nonzero tensor components are

$$\begin{aligned}
\mathbf{T}_0^{(1,-1)} &= -\frac{1}{2}\sqrt{\frac{3}{5}}, \\
\mathbf{T}_0^{(2,+1)} &= \frac{1}{2}\sin 2\chi, \\
\mathbf{T}_{\pm 2}^{(2,-1)} &= \pm\frac{1}{2\sqrt{6}} e^{\pm 2i\psi}\cos 2\chi, \\
\mathbf{T}_0^{(3,-1)} &= -\frac{1}{\sqrt{10}}, \\
\mathbf{T}_{\pm 2}^{(3,-1)} &= \frac{1}{2\sqrt{3}} e^{\pm 2i\psi}\cos 2\chi.
\end{aligned}$$

In particular, $\mathbf{T}_{\pm 3}^{(3,-1)} = 0$.

We proved that the action of Θ on the system can be replaced by its action on $\mathbf{T}_{\beta}^{(b,\theta)}$, which was found to be

$$\Theta \mathbf{T}_{\beta}^{(b,\theta)} = \theta \mathbf{T}_{\beta}^{(b,\theta)}.$$

This result is nontrivial because the action of the time-reversal operator Θ on a spherical tensor is usually described by

$$\mathbf{T}_m^{(j)} \to (-1)^{j-m} \mathbf{T}_{-m}^{(j)}$$

(see [30, 33]) or

$$\Theta \mathbf{T}_m^{(j)} = (-1)^m \mathbf{T}_{-m}^{(j)}$$

(see [31]). Here, the result is different because the time-reversal operator does not act directly on the spherical tensor. Its action on the system is translated into a simpler action on the polarization and wave vectors.

More generally, any symmetry operation S acting on the system can be written as

$$S = I^p \Theta^t R T_{\mathbf{R}},$$

where $p = 1$ or $p = 0$ if S contains or does not contain the inversion, $t = 1$ or $t = 0$ if S contains or does not contain the time-reversal symmetry, R denotes a rotation and $T_{\mathbf{R}}$ a translation. From the identity $\sigma(\epsilon, \mathbf{k}; I) = \sigma(-\epsilon, -\mathbf{k})$, we see that the action of the parity operator on the system reverses the $E1E2$ absorption cross section (i.e., $\sigma_{E1E2}(I) = -\sigma_{E1E2}$). Therefore, the action of a general symmetry operation S on the system transforms σ_{E1E2} into

$$\begin{aligned}
\sigma_{E1E2}(S) = \sum_{b=1}^{3} \sum_{\beta=-b}^{b} (-1)^{\beta} \times \\
\times \sum_{\theta=\pm 1} (-1)^{p\theta^t} \mathbf{D}_{\beta'\beta}^{(b)}(R) \mathbf{T}_{\beta'}^{(b,\theta)}\, \sigma_{-\beta}^{(b,\theta)}, \qquad (5)
\end{aligned}$$

where $\mathbf{D}_{\beta'\beta}^{(b)}(R)$ is the Wigner rotation matrix. This result justifies the use of the character method, which was employed by Tenenbaum in Ref. [34] and which we use in Sec. 3.

For a magnetic group G_M containing g_m elements, the form of the absorption cross section is obtained by taking the average over the elements of the group,

$$\langle \sigma_{E1E2} \rangle = \sum_{b=1}^{3} \sum_{\beta=-b}^{b} (-1)^{\beta} \sum_{\theta=\pm 1} \langle \mathbf{T}_{\beta}^{(b,\theta)} \rangle\, \sigma_{-\beta}^{(b,\theta)}, \qquad (6)$$

where

$$\langle \mathbf{T}_{\beta}^{(b,\theta)} \rangle = \frac{1}{g_m} \sum_{S \in G_M} (-1)^{p\theta^t} \mathbf{D}_{\beta'\beta}^{(b)}(R) \mathbf{T}_{\beta'}^{(b,\theta)}.$$

2.4. Effective operators of XOA

2.4.1. Spherical basis

The $E1E2$ sum rules were calculated by Carra and collaborators using the powerful method of group generators [27, 35–37]. A key achievement was to show that all operators $\mathbf{\Sigma}^{(b,\theta)}$ can be built from the triad of mutually orthogonal vector operators:

1) $\mathbf{n} = \mathbf{r}/r$, which is a time-reversal even, polar vector typically associated with the electric dipole moment;

2) the orbital angular momentum $\mathbf{L}$, which is a time-reversal odd axial vector;

3) the toroidal vector $\mathbf{\Omega} = [(\mathbf{n} \times \mathbf{L}) - (\mathbf{L} \times \mathbf{n})]/2$, which is odd with respect to both I and Θ.

Because $\mathbf{\Omega}$ can be rewritten as the commutator, $\mathbf{\Omega} = i\left[\mathbf{n}, \mathbf{L}^2\right]/2$, we show in Sec. 3 that it is proportional to the orbital anapole moment defined in [2].

Important results heve been established.

1) The XMχD sum rule involves the ground state expectation value of the toroidal vector $\mathbf{\Omega}^{(1,-1)}$ projected along the direction of the wave vector $\mathbf{k}$.

2) The XNCD sum rule must yield the expectation value of the Θ-even pseudodeviator $\mathbf{N}^{(2,+1)} = [\mathbf{L}, \mathbf{\Omega}]^{(2)}$, which is obtained for $a = 1$, $b = 2$.

3) For $a = b = 2$, the effective operator must be a Θ-odd pseudodeviator, which was identified with $\mathbf{W}^{(2,-1)} = [\mathbf{L}, \mathbf{n}]^{(2)}$. Its ground state expectation value appears in the nonreciprocal XMLD sum rule.

4) For $a = 2$ and $b = 3$, the effective operator is the Θ-odd septor $\mathbf{\Gamma}^{(3,-1)} = \left[[\mathbf{L}, \mathbf{L}]^{(2)}, \mathbf{\Omega}\right]^{(3)}$. Its ground state expectation value is involved in the XMχD sum rule and in the nonreciprocal XMLD sum rule.

As long as the definition of the polarization tensors $\mathbf{T}_{\beta}^{(b,\theta)}$ given in the previous section is applicable, we can use the following generic formulations of the XOA sum rules, to be called the Carra–Jerez–Marri equations hereafter [37]:

for XNCD (S_3),

$$\Sigma_{E1E2} = \frac{-8\pi^2\alpha}{3\hbar c}\sin 2\chi\,(2\ell_c+1)\sum_{\ell,\ell'} R_{\ell}^{(1)} R_{\ell'}^{(2)} \times \\ \times\, a^{(2,+1)}(\ell_c,\ell,\ell')\sqrt{\frac{3}{2}}\left\langle \mathbf{N}_0^{(2,+1)}(\ell,\ell')\right\rangle, \quad (7)$$

for XMχD (S_0),

$$\Sigma_{E1E2} = \frac{-2\pi^2\alpha}{\hbar c}(2\ell_c+1)\sum_{\ell,\ell'} R_{\ell}^{(1)} R_{\ell'}^{(2)} \times \\ \times\left\{\frac{2}{5}a^{(1,-1)}(\ell_c,\ell,\ell')\left\langle \mathbf{\Omega}_0^{(1,-1)}(\ell,\ell')\right\rangle - \right. \\ \left. - \frac{16}{\sqrt{10}}b^{(3,-1)}(\ell_c,\ell,\ell')\left\langle \Gamma_0^{(3,-1)}(\ell,\ell')\right\rangle\right\}, \quad (8)$$

for XMLD (S_1, S_2),

$$\Sigma_{E1E2} = \frac{16\pi^2\alpha\cos 2\chi}{\hbar c}(2\ell_c+1)\sum_{\ell,\ell'} R_{\ell}^{(1)} R_{\ell'}^{(2)} \times \\ \times\sum_{\beta=\pm 2}\left\{a^{(2,-1)}(\ell_c,\ell,\ell')\frac{ie^{i\beta\psi}}{3\beta}\left\langle \mathbf{W}_{\beta}^{(2,-1)}(\ell,\ell')\right\rangle + \right. \\ \left. + \frac{e^{i\beta\psi}}{\sqrt{3}}b^{(3,-1)}(\ell_c,\ell,\ell')\left\langle \Gamma_{\beta}^{(3,-1)}(\ell,\ell')\right\rangle\right\}. \quad (9)$$

In these equations, $R_{\ell}^{(1)}$and $R_{\ell'}^{(2)}$ denote the radial dipole and quadrupole integrals that are classically defined as

$$R_{\ell}^{(1)} = \int_0^{\rho_{MT}} r^3 dr \phi_c(r)\,\varphi_{\ell}(r),$$

$$R_{\ell'}^{(2)} = \int_0^{\rho_{MT}} r^4 dr \phi_c(r)\,\varphi_{\ell'}(r),$$

where the core state and photoelectron radial wave functions are $\phi_c(r)$ and $\varphi_{\ell,\ell'}$, respectively; $\phi_c(r)$ is typically localized in a muffin-tin sphere of the radius ρ_{MT}. The expressions for the numerical factors $a^{(2,+1)}$, $a^{(2,-1)}$, $a^{(1,-1)}$, $b^{(3,-1)}$ are given in Table 2.

2.4.2. Cartesian basis

For linear dichroism experiments, it is more appropriate to express Eq. (9) in terms of Hermitian Cartesian effective operators. This can easily be done using the relations (see, e.g., Refs. [22, 38])

$$\mathbf{W}_{\pm 2}^{(2,-1)} = \frac{1}{2}\left[W_{XX}^{(2,-1)} - W_{YY}^{(2,-1)}\right] \pm \\ \pm\frac{1}{2}\left[W_{XY}^{(2,-1)} + W_{YX}^{(2,-1)}\right],$$

$$\mathbf{\Gamma}_{\pm 2}^{(2,-1)} = \frac{\sqrt{3}}{2}\left[\Gamma_{XXZ}^{(3,-1)} - \Gamma_{YYZ}^{(3,-1)}\right] \pm \\ \pm\frac{\sqrt{3}}{2}\left[\Gamma_{XYZ}^{(3,-1)} + \Gamma_{YXZ}^{(3,-1)}\right],$$

where $\{X, Y, Z\}$ are Cartesian coordinates in the reference frame used to define the polarization tensors in Subsec. 2.3.2. Hence, the two effective operators defined in Eq. (9) can now be rewritten as

$$i\left[e^{2i\psi}\left\langle \mathbf{W}_{+2}^{(2,-1)}\right\rangle - e^{-2i\psi}\left\langle \mathbf{W}_{-2}^{(2,-1)}\right\rangle\right] = \\ = \sin 2\psi\left[\left\langle W_{YY}^{(2,-1)}\right\rangle - \left\langle W_{XX}^{(2,-1)}\right\rangle\right] - \\ - \cos 2\psi\left[\left\langle W_{XY}^{(2,-1)}\right\rangle + \left\langle W_{YX}^{(2,-1)}\right\rangle\right], \quad (10)$$

$$\left[e^{2i\psi}\left\langle \mathbf{\Gamma}_{+2}^{(3,-1)}\right\rangle + e^{-2i\psi}\left\langle \mathbf{\Gamma}_{-2}^{(3,-1)}\right\rangle\right] = \\ = \sin 2\psi\left[\left\langle \Gamma_{XYZ}^{(3,-1)}\right\rangle + \left\langle \Gamma_{YXZ}^{(2,-1)}\right\rangle\right] - \\ - \cos 2\psi\left[\left\langle \Gamma_{YYZ}^{(3,-1)}\right\rangle - \left\langle \Gamma_{XXZ}^{(3,-1)}\right\rangle\right]. \quad (11)$$

Because

$$S_1/S_0 = \cos 2\chi\cos 2\psi, \quad S_2/S_0 = \cos 2\chi\sin 2\psi,$$

Table 2. Numerical factors

$$a^{(1,-1)}(l_c,l,l') = \frac{(l_c+l+1)(l_c+l-2l')(l_c+2l'-l+1)}{(l_c+l)(l_c+l+2)(l+l'+1)^2}$$

$$a^{(2,+1)}(l_c,l,l') = \frac{2(2l+1)(2l'+1)[6+3l_c(l_c+1)-2l(l+1)-l'(l'+1)]}{(l+l'+1)(l_c-3l'+2l)(l_c+3l'-2l+1)(l_c+l)^2(l_c+l+2)^2}$$

$$a^{(2,-1)}(l_c,l,l') = \frac{(l'-l)(2l+1)(2l'+1)[6+3l_c(l_c+1)-2l(l+1)-l'(l'+1)]}{2(l_c-3l'+2l)(l_c+3l'-2l+1)(l_c+l)^2(l_c+l+2)^2}$$

$$b^{(3,-1)}(l_c,l,l') = \frac{2(2l+1)(2l'+1)}{(l+l'+1)(l_c-3l'+2l)(l_c+3l'-2l+1)(l_c+l)^2(l_c+l+2)^2}$$

it becomes obvious that within the defined reference frame, $\left[W_{YY}^{(2,-1)} - W_{XX}^{(2,-1)}\right]$ is the effective operator responsible for the Jones dichroism XMLD (S_2), and $\left[W_{XY}^{(2,-1)} + W_{YX}^{(2,-1)}\right]$ is the effective operator of XMLD (S_1). It can be seen that the septor terms $\left[\Gamma_{XYZ}^{(3,-1)} + \Gamma_{YXZ}^{(3,-1)}\right]$ and $\left[\Gamma_{YYZ}^{(3,-1)} - \Gamma_{XXZ}^{(3,-1)}\right]$ also contribute to XMLD (S_2) and XMLD (S_1), respectively. Typically, the contributions of $\left[W_{YY}^{(2,-1)} - W_{XX}^{(2,-1)}\right]$ and $\left[\Gamma_{YYZ}^{(3,-1)} - \Gamma_{XXZ}^{(3,-1)}\right]$ are in quadrature with respect to the angular dependence 2ψ.

Identical conclusions can be reached by directly decomposing the rank-3 gyration tensor $\zeta_{\alpha\beta\gamma}$ into rotational invariants following procedures reviewed in [22]. Such a decomposition yields one scalar $\left(\zeta^{(0)}\right)$, three vectors $\left(\zeta_\gamma^{(1)}\right)$, two deviators $\left(\zeta_{\alpha\beta}^{(2)}\right)$, and one septor $\left(\zeta_{\alpha\beta\gamma}^{(3)}\right)$. Because the $E1E2$ interference terms have no scalar part, it follows that $\left(\zeta^{(0)}\right) = 0$. Regarding the vector components, it follows from Sec. 2.2 that only the vector part collinear with k_γ is involved, i.e., $\zeta_\gamma^{(1)\prime} = \delta_{\alpha\beta}\zeta'_{\alpha\beta\gamma}$. Therefore, $\zeta_\gamma^{(1)}$ must be identified with the expectation value of the anapole component $\left\langle \Omega_\gamma^{(1,-1)} \right\rangle = \left\langle \mathbf{\Omega}_0^{(1,-1)} \right\rangle$.

Two pseudodeviators can be generated by a symmetric contraction of $\zeta'_{\alpha\beta\gamma}$[22]:

$$\left[\zeta_{\alpha\beta}^{\prime(2)}\right]_1 = -\frac{1}{2}\left[\epsilon_{\alpha ij}\zeta'_{ji\beta} + \epsilon_{\beta ij}\zeta'_{ji\alpha}\right],$$

$$\left[\zeta_{\alpha\beta}^{\prime(2)}\right]_2 = -\frac{1}{2}\left[\epsilon_{ji\beta}\zeta'_{\alpha ij} + \epsilon_{ji\alpha}\zeta'_{\beta ij}\right].$$

Given the symmetry properties of the gyration tensor, we can check that $\left[\zeta_{\alpha\beta}^{\prime(2)}\right]_1 = 0$, and therefore

$$\left[\zeta_{\alpha\beta}^{\prime(2)}\right]_2 \propto \left\langle W_{\alpha\beta}^{(2,-1)} \right\rangle.$$

In Sec. 3, we address the inverse problem: assuming that we know some physical realization of a rank-2 irreducible tensor $\left\langle W_{\alpha\beta}^{(2,-1)} \right\rangle$, we can generate its embedded form in the rank-3 tensor space [22],

$$\zeta_{\alpha\beta\gamma}^{\prime(2)} \propto 2\epsilon_{\alpha\beta\delta}\left\langle W_{\delta\gamma}^{(2,-1)} \right\rangle + \epsilon_{\delta\beta\gamma}\left\langle W_{\alpha\delta}^{(2,-1)} \right\rangle,$$

$$\zeta_{\alpha\beta\gamma}^{\prime\prime(2)} \propto 2\epsilon_{\alpha\beta\delta}\left\langle N_{\delta\gamma}^{(2,+1)} \right\rangle + \epsilon_{\delta\beta\gamma}\left\langle N_{\alpha\delta}^{(2,+1)} \right\rangle.$$

Keeping in mind that $\zeta_{\alpha\beta\gamma}^{\prime(2)}$ must be symmetric and $\zeta_{\alpha\beta\gamma}^{\prime\prime(2)}$ must be antisymmetric under the transposition of the α,β subscripts, we finally obtain after proper symmetrization that
for XMLD (S_1),

$$\left[\zeta_{\beta\beta\gamma}^{\prime(2)} - \zeta_{\alpha\alpha\gamma}^{\prime(2)}\right] \propto \left[\left\langle W_{\alpha\beta}^{(2,-1)} \right\rangle + \left\langle W_{\beta\alpha}^{(2,-1)} \right\rangle\right];$$

for XMLD (S_2),

$$\left[\zeta_{\alpha\beta\gamma}^{\prime(2)} + \zeta_{\beta\alpha\gamma}^{\prime(2)}\right] \propto \left[\left\langle W_{\alpha\alpha}^{(2,-1)} \right\rangle - \left\langle W_{\beta\beta}^{(2,-1)} \right\rangle\right],$$

for XNCD (S_3),

$$\left[\zeta_{\alpha\beta\gamma}^{\prime\prime(2)} - \zeta_{\beta\alpha\gamma}^{\prime\prime(2)}\right] \propto \left\langle N_{\gamma\gamma}^{(2,+1)} \right\rangle.$$

On the other hand, the septor $\Gamma_{\alpha\beta\gamma}^{(3,-1)}$ must be the natural irreducible representation of the rank-3 tensor $\zeta'_{\alpha\beta\gamma}$. It is expected to contribute to both XMLD (S_1) and XMLD (S_2) because

$$\left[\zeta_{\beta\beta\gamma}^{\prime(3)} - \zeta_{\alpha\alpha\gamma}^{\prime(3)}\right] \propto \left[\Gamma_{\beta\beta\gamma}^{(3,-1)} - \Gamma_{\alpha\alpha\gamma}^{(3,-1)}\right],$$

$$\left[\zeta_{\alpha\beta\gamma}^{\prime(3)} + \zeta_{\beta\alpha\gamma}^{\prime(3)}\right] \propto \left[\Gamma_{\alpha\beta\gamma}^{(3,-1)} + \Gamma_{\beta\alpha\gamma}^{(3,-1)}\right].$$

The two approaches are indeed equivalent.

3. PHYSICAL IMPLICATIONS

3.1. Orbital magnetoelectric operators

3.1.1. Spin and orbital anapoles

As was first pointed out by Zel'dovich [1], a toroidal solenoid generates not only an annular magnetic field $\mathbf{H}_a(\mathbf{r})$, but also the so-called toroidal current $\mathbf{j}_a(\mathbf{r})$ along the torus axis z [1–3, 39]. The anapole moment $\mathbf{A}$ is defined as the root-mean-square (rms) radius of $\mathbf{j}_a(\mathbf{r})$. As emphasized long ago in [5], one should not confuse the anapole moment with the toroidal dipole moment $\mathbf{M}_{td}$ in the theory of classical electrodynamics [7]. Khriplovich [2] and others [40] have nevertheless proved that in a stationary state, where $\mathbf{j}_a(\mathbf{r})$ is time-independent, the two moments become equivalent up to the factor 4π, i.e.,

$$\mathbf{A} = 4\pi \mathbf{M}_{td}.$$

We use this equivalence in Sec. 4 because the current literature on magnetoelectric solids mostly refers to toroidal dipole moment.

In solid state physics, annular magnetic fields can be associated with either spin or orbital currents. The magnetoelectric character of a spin anapole [42] is schematically illustrated in Fig. 1. In the presence of a magnetic field $\mathbf{H}$, the energy of each spin carrier (electron) depends on its location on the annular orbit to which the electrons are constrained: their distribution is no longer uniform; consequently, an electric polarization $\mathbf{P}$ is generated in the direction that is mutually orthogonal to $\mathbf{H}$ or $\mathbf{j}_a(\mathbf{r})$. The case of an orbital anapole was also envisaged by Ginzburg, Gorbatsevich, Kopaev and their collaborators [8] many years ago, but in a different theoretical perspective.

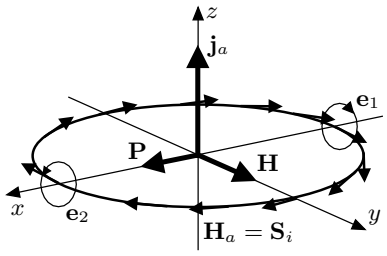

Fig. 1. Magnetoelectric character of a spin anapole: in an external magnetic field $\mathbf{H}$, the electron distribution is no longer uniform and induces an electric polarization orthogonal to $\mathbf{H}$

Following [2] or [43], we can decompose the total anapole moment into its spin and orbital components,

$$\left\langle \mathbf{A}_{spin}^{(1,-1)} \right\rangle = 2\pi\mu_B \sum_i \langle \mathbf{S}_i \times \mathbf{r}_i \rangle , \qquad (12)$$

$$\left\langle \mathbf{A}_{orb}^{(1,-1)} \right\rangle = -i\frac{2\pi\mu_B}{3} \sum_i \left\langle \left[\mathbf{L}_i^2, \mathbf{r}_i\right] \right\rangle = \\ = \frac{2\pi\mu_B}{3} \left\langle \mathbf{\Omega}^{(1,-1)} \right\rangle , \qquad (13)$$

where it can be checked that the operator $-i\left[\mathbf{L}^2, \mathbf{r}\right]$ is both Hermitian and Θ-odd [43]. We immediately obtain that

$$\mathbf{M}_{td}^{orb} = \frac{\mu_B \langle \mathbf{\Omega} \rangle}{6}.$$

At this stage, we must recall Lloyd's theorem, which states that for (diamagnetic) systems that have an even number of electrons and integral spin, the expectation value of Hermitian Θ-odd operators vanishes [43].

3.1.2. Operators conserved by $I\Theta$

We now consider the perturbation of a system that is in a remanent magnetoelectric state, when one electron is annihilated in a core state and one electron $\{\mathbf{n}, \mathbf{L}, \mathbf{S}\}$ is created in a virtual ground state. By analogy with [44], we expand the energy $U(n, L, S)$ into a MacLaurin series [27]. Using a Cartesian basis, we obtain

$$U(n, L, S) = U(0, 0, 0) + \\ + \sum_m \left\{ \frac{1}{m!} [n_\alpha \partial_{n_\alpha} + L_\beta \partial_{L_\beta} + S_\beta \partial_{S_\beta}]^m U(0, 0, 0) \right\}. \qquad (14)$$

We need to retain only the magnetoelectric interference terms that are invariant in the product $I\Theta$ and contribute to the nonreciprocal XOA. In the case of a K-shell ionization, the spin does not play any role and can be neglected. Starting with $m = 2$, we obtain a rank-2 Cartesian tensor $[a_{\alpha\beta}]_{orb}$ that is the ground state expectation value of the orbital part of the one-electron magnetoelectric tensor associated with the dyad $[L \otimes n]$. Indeed, we can decompose $[a_{\alpha\beta}]_{orb}$ into its irreducible representations, which include a pseudoscalar (i.e., the trace), the dual vector of the antisymmetric part, and the traceless pseudodeviator of the totally symmetric part. It is then straightforward to show that the integrated XMχD signal, via the expectation value of the orbital anapole moment, is proportional to the dual vector of $[a_{\alpha\beta}]_{orb}$,

$$\Sigma_{XM\chi D\ (S_0)} \propto \left\langle \Omega_\gamma^{(1,-1)} \right\rangle \propto \frac{1}{2} \epsilon_{\alpha\beta\gamma} [a_{\alpha\beta}]_{orb} .$$

We note that this is a direct transposition of the result established long time ago by Ascher [39] and by Gorbatsevich et al. [41, 42], who pointed out that for a toroidal magnetoelectric solid, the total anapole moment $\langle A_{total}\rangle$ is proportional to the dual vector of the rank-2 magnetoelectric tensor $[a_{\alpha\beta}]$, i.e.,

$$\langle A_\gamma\rangle \propto \frac{1}{2}\epsilon_{\alpha\beta\gamma}\,[a_{\alpha\beta}]\,.$$

We also show that at the $m=2$ order, $\Sigma_{XMLD}(S_1)$ and $\Sigma_{XMLD}(S_2)$ can similarly be related to the irreducible zero-trace symmetric pseudodeviator $[a_{\alpha\beta}]^{(2)}_{orb}$ because we have seen that

$$\left[\left\langle W^{(2,-1)}_{\alpha\beta}\right\rangle + \left\langle W^{(2,-1)}_{\beta\alpha}\right\rangle\right] \propto [a_{\alpha\beta}+a_{\beta\alpha}]_{orb},$$

$$\left[\left\langle W^{(2,-1)}_{\alpha\alpha}\right\rangle - \left\langle W^{(2,-1)}_{\beta\beta}\right\rangle\right] \propto [a_{\alpha\alpha}-a_{\beta\beta}]_{orb}.$$

This implies that XMLD (S_1) and the Jones dichroism XMLD (S_2) are also first-order magnetoelectric effects, but of the orbital nature. Typically, XMLD (S_2) can be detected in magnetoelectric solids characterized by a magnetoelectric tensor that has nonzero diagonal terms. More precisely, this dichroism should be observed whenever the diagonal terms are not equal in the plane $(0,0,k)$. The dichroism XMLD (S_1) is expected to be detectable only when the magnetoelectric tensor has symmetric off-diagonal terms, a situation which is less frequent.

At the K-edge, there is no hope to access the spin part of the one-electron magnetoelectric tensor $[S\otimes n]$, which can also be decomposed into the spin anapole $A^{(1,-1)}_{spin}$ and the pseudodeviator $A^{(2,-1)}_{spin}$. *A priori*, nothing can be said about the relative sign and magnitude of the spin and orbital parts of the total magnetoelectric tensor. At most, it may be guessed that for transition metal oxides, the spin part $[a_{\alpha\beta}]_{spin}$ should be much larger than the orbital part $[a_{\alpha\beta}]_{orb}$. To date, magnetoelectric susceptibility measurements were largely dominated by the spin contribution, and to the best of our knowledge, there is not a single example where the orbital part has been extracted. What makes X-ray absorption spectroscopy attractive is indeed its capability to probe the orbital contributions to the magnetoelectric tensor selectively.

At the $m=4$ order, additional magnetoelectric interference terms can be identified that are odd with respect to parity I and time-reversal Θ but remain invariant under the product $I\Theta$. Such terms can only be obtained from the two rank-4 Cartesian tensors

$$[b_{\beta\gamma\delta\epsilon}]_{orb} = [L\otimes L\otimes L\otimes n]\,,$$

$$[c_{\beta\gamma\delta\epsilon}]_{orb} = [L\otimes n\otimes n\otimes n]\,.$$

We recall that the rank-4 tensor $[L\otimes n\otimes L\otimes n]$, which contributes to the so-called biquadratic susceptibility [45], is obviously parity-even and cannot therefore contribute to XOA. As far as XOA is concerned, we must only retain irreducible tensors of rank ≤ 3 that are linear with respect to n. We are then left with (at most) three independent Cartesian septors obtained by decomposing $[b_{\beta\gamma\delta\epsilon}]_{orb}$ into irreducible representations. The latter are related to the six dual rank-3 tensors generated by antisymmetric contraction [22], i.e.,

$${}_\tau t_{\alpha\beta\gamma} \propto \epsilon_{\alpha\delta\epsilon}\,[b_{\beta\gamma\delta\epsilon}]_{orb}\,,$$

with τ varying from 1 to 6. Three independent tensors are easily identified,

$${}_1\Gamma_{\alpha\beta\gamma} = [L\otimes L\otimes\Omega]_{\alpha\beta\gamma} = \left[Q^{(2,+1)}_{LL}\otimes\Omega^{(1,-1)}\right]_{\alpha\beta\gamma},$$

$${}_2\Gamma_{\alpha\beta\gamma} = [\Pi_{LL}\otimes L\otimes n]_{\alpha\beta\gamma} = \left[\Pi^{(1,+1)}_{LL}\otimes W^{(2,-1)}\right]_{\alpha\beta\gamma},$$

$${}_3\Gamma_{\alpha\beta\gamma} = [L\otimes\Pi_{LL}\otimes n]_{\alpha\beta\gamma}\,,$$

where

$$\left[\Pi^{(1,+1)}_{LL}\right]_\gamma = [L\times L]_\gamma = iL_\gamma$$

can be viewed as an example of an antitoroidal vector operator that is not Hermitian. As a consequence, only the expectation value of the first septor operator is real and can contribute to XOA. At this stage, it becomes more convenient to return to the representation in the spherical basis. We first observe that for the septor

$$\left\langle \mathbf{\Gamma}^{(3,-1)}_0\right\rangle = \left\langle \mathbf{Q}^{(2,+1)}_{LL}, \mathbf{\Omega}^{(1,-1)}\right\rangle$$

to exist, it is sufficient but not necessary that $\langle\mathbf{\Omega}\rangle$ and $\langle\mathbf{Q}_{LL}\rangle \neq 0$ individually. We note that the tensor $\mathbf{Q}^{(2,+1)}_{LL}$, which is Θ- and I-even, has the same symmetry and angular dependence as the charge quadrupole operator, although the matrix elements are different. Interestingly, $\mathbf{Q}^{(2,+1)}_{LL}$ was recently shown [46, 47] to be also the effective operator responsible for the reciprocal X-ray magnetic linear dichroism (XMLD) of a magneto-optical origin [48].

At this stage, it can be anticipated that in analyzing XMχD spectra, we could experience serious difficulties in disentangling the contributions of $\mathbf{\Gamma}^{(3,-1)}_0$ and $\mathbf{\Omega}^{(1,-1)}_0$, especially if these two operators appearing in Eq. (8) are both allowed by symmetry. In principle, the higher-order septor term can be expected to be smaller. As discussed in Sec. 3.3.2 below, comparison of the XMχD spectra recorded with a single crystal or a powder can be very helpful in verifying the

Table 3. X-ray optically active magnetoelectric group $G_{mag}[\chi_\Omega, \chi_W, \chi_\Gamma]$

Anapole		$\mathbf{\Omega}^{(1)} \neq 0$		$\mathbf{\Omega}^{(1)} = 0$	
Deviator		$\mathbf{W}^{(2)} = 0$	$\mathbf{W}^{(2)} \neq 0$	$\mathbf{W}^{(2)} \neq 0$	
Septor		$\mathbf{\Gamma}^{(3)} \neq 0$		$\mathbf{\Gamma}^{(3)} = 0$	$\mathbf{\Gamma}^{(3)} \neq 0$
AFM	AFE	$\bar{3}'m[1,0,2]$ $4/m'mm[1,0,1]$ $\bar{4}'2'm[1,0,1]$ $6/m'mm[1,0,1]$ $\bar{6}'2'm[1,0,1]$	$\bar{1}'[3,5,7]$; $mmm'[1,1,2]$ $2/m'[1,3,3]$; $2'/m[2,2,4]$ $\bar{3}'[1,1,3]$ $\bar{4}'[1,1,1]$; $4/m'[1,1,1]$ $\bar{6}'[1,1,1]$; $6/m'[1,1,1]$	$4/m'm'm'[0,1,0]$ $422[0,1,0]$ $\bar{4}'2m'[0,1,0]$ $\bar{4}'m'2[0,1,0]$ $622[0,1,0]$ $\bar{6}'2m'[0,1,0]$ $\bar{4}'m'2[0,1,0]$	$222[0,2,1]$ $m'm'm'[0,2,1]$ $4'/m'[0,2,2]$ $4'/m'mm'[0,1,1]$ $4'mm'[0,1,1]$ $\bar{4}2m[0,1,1]$ $\bar{4}2'm'[0,1,1]$ $32[0,1,1]$ $\bar{3}'m'[0,1,1]$
AFM	FE	$3m[1,0,2]$ $4mm[1,0,1]$; $6mm[1,0,1]$	$mm2[1,1,2]$ $(2mm)^*[1,1,2]$ $(m2m)^*[1,1,2]$		$4'[0,2,2]$
FM	AFE	$32'[1,0,2]$ $42'2'[1,0,1]$; $62'2'[1,0,1]$			$\bar{4}[0,2,2]$
FM	FE		$3[1,1,3]$ $4[1,1,1]$; $6[1,1,1]$	$4m'm'[0,1,0]$ $6m'm'[0,1,0]$	$m'm'2[0,2,1]$ $3m'[0,1,1]$
Weak FM	AFE		$22'2'[1,1,2]$ $(2'22')^*[1,1,2]$; $(2'2'2)^*[1,1,2]$		
Weak FM	FE		$1[3,5,7]$; $2[1,3,3]$; $2'[2,2,4]$ $m[2,2,4]$; $m'[1,3,3]$ $m'm2'[1,1,2]$; $mm'2'[1,1,2]$		

* Non-standard groups.

validity of this assumption. We assume that we can perform XMLD (S_2) experiments with a single crystall; Eqs. (9)–(11) show that the effective operators $\left[W_{YY}^{(2,-1)} - W_{XX}^{(2,-1)}\right]$ and $\left[\Gamma_{YYZ}^{(2,-1)} - \Gamma_{XXZ}^{(2,-1)}\right]$ have the same angular dependence (2ψ) when the crystal is rotated around the direction of the incident X-ray beam, but we already pointed out that the two contributions are in quadrature. This implies that the higher-order septor must induce only a small phase shift with respect to the dominant XMLD (S_2) signal. The same conclusion must obviously be true for nonreciprocal XMLD (S_1) experiments. Again, the comparison of nonreciprocal XMLD spectra recorded with a single crystal or a powdered sample could be most helpful in evaluating the importance of the septor term. This option is also considered in Sec. 3.3.2.

In Table 3, we have summarized the effective XOA operators that are irreducible representations of a given magnetoelectric point group. Table 3 is a spin-off of the work of Tenenbaum [34] who listed the number of independent components of the spherical tensors up to rank 4 for 90 magnetic point groups. We recall, however, that this application was justified in Sec. 2.3.2. For each magnetoelectric class, we indicated the number of independent, nonzero components of the anapole ($\chi_\Omega \leq 3$), of the pseudodeviator $\mathbf{W}^{(2,-1)}(\chi_W \leq 5)$, and of the pseudoseptor $\Gamma^{(3,-1)}(\chi_\Gamma \leq 7)$. We have identified 34 «toroidal point groups» (but only 31 classes) [6, 39] that admit the anapole as an irreducible representation and we found that all of them also admit $\mathbf{\Gamma}^{(3)}$ as an irreducible representation. We have also found 22 «nontoroidal groups» that admit the pseudodeviator $\mathbf{W}^{(2,-1)}$ as an irreducible representation and may exhibit nonreciprocal XMLD; interestingly, 13 of them still admit the pseudoseptor $\mathbf{\Gamma}^{(3,-1)}$ as an irreducible representation. Not listed in Table 3 are the magnetic classes that are not magnetoelectric but still admit $\mathbf{\Gamma}^{(3)}$ as irreducible representations,

Table 4. Operators for induced magnetoelectric susceptibilities

$I=-1,\ \Theta=+1\ (HHE)$ $E1E2$ compatible	$I=+1,\ \Theta=-1\ (EEH)$ $E2E2 + E1E3$ compatible
Piezo-electric	Piezo-magnetic
$[\mathbf{L}\cdot\mathbf{\Omega}]^{(0)}$ $[\mathbf{L}\times\mathbf{\Omega}-\mathbf{\Omega}\times\mathbf{L}]^{(1)}$ $[\mathbf{L},\mathbf{\Omega}]^{(2)}$ $[\mathbf{L},\mathbf{W}^{(2)}]^{(3)}$	$[\mathbf{n}\cdot\mathbf{\Omega}]^{(0)}$ $[\mathbf{n}\times\mathbf{\Omega}-\mathbf{\Omega}\times\mathbf{n}]^{(1)}$ $[\mathbf{n},\mathbf{\Omega}]^{(2)}$ $[\mathbf{n},\mathbf{W}^{(2)}]^{(3)}$

$$6';\overline{6};6'/m;6'22';6'mm';\overline{6}m2;6'/mmm';$$

$$23;m'3;m'3m;4'32;\overline{4}3m.$$

For nonreciprocal XOA to be detectable, the orbital magnetoelectric group must imperatively belong to the groups listed in Table 3. This is not sufficient, unfortunately, because Table 3 does not tell us whether the specific representations $\mathbf{W}^{(2,-1)}_{(\pm2)}$ and $\mathbf{\Gamma}^{(3,-1)}_{(0,\pm2)}$ are allowed. This is where Eq. (6) has to be used. In the specific case of the Jones dichroism, one can alternatively exploit the fact that the Cartesian tensors $W^{(2,-1)}_{\alpha\beta}$ must have the same form as the magnetoelectric tensors in [49] or [50]: using Eq. (10), it is then a trivial exercise to identify which magnetoelectric groups give a nonreciprocal dichroism XMLD (S_2).

3.1.3. Operators not conserved by $I\Theta$

The so-called higher-order magnetoelectric effects, or the induced magnetoelectric effects in paramagnetic systems [51], are commonly associated with rank-3 susceptibility tensors referring to $H_\alpha H_\beta E_\gamma$ or $E_\alpha E_\beta H_\gamma$ [52]. The corresponding tensors are therefore odd with respect to $I\Theta$ and can be identified with cross terms in the MacLaurin expansion of the energy U at the intermediate order ($m=3$). As pointed out in [52], these additional terms must be taken into consideration for magnetic groups that are compatible with either piezomagnetism or piezoelectricity. Neither the group $\overline{3}'m'$ of Cr_2O_3 nor the groups $2/m'$ and $2'/m$ to be considered in Sec. 4 for $(V_{1-x}Cr_x)_2O_3$ belong to these classes, but we nevertheless feel useful to look at the relevant effective operators listed in Table 4.

Because we are primarily interested in the σ_{E1E2} X-ray absorption cross section, we first consider the case of the odd parity HHE susceptibilities. The Hermitian operators listed in the first column of Table 4 can be seen as describing magnetic field-induced magnetoelectric properties. It immediately appears, however, that the first 3 operators in the first column are the effective operators for natural optical activity as discussed in more detail in Sec. 3.2. Of particular importance is the scalar term, which is a parity-violating energy of orbital origin but is fully consistent with the formulation in [1]. For example, in a population of resolved chiral species in a disordered fluid phase, each enantiomer must bear an orbital anapole moment with a well-defined sign in the molecular coordinate system, but because the orientation of molecules is random in a disordered fluid phase, there is obviously no magnetochiral dichroism that can be detected. In the presence of a strong external field $\mathbf{H}$, the magnetoelectric energy of the system becomes

$$[\mathbf{L}\cdot\mathbf{\Omega}]_{\mathbf{H}}=[\mathbf{L}_0\cdot\mathbf{\Omega}_0]+[\chi_{orb}\mathbf{H}\cdot\mathbf{\Omega_0}]+[\mathbf{L}_0\cdot\Delta\mathbf{\Omega_H}]+\ldots$$

where

$$\mathbf{L}=\mathbf{L}_0+\chi_{orb}\mathbf{H}.$$

Neglecting the field-induced anapole moment $\Delta\Omega_H$ in the first approximation, we expect the system to minimize its magnetoelectric energy with an anisotropic angular distribution of the anapole preferably oriented along the direction of the external magnetic field $\mathbf{H}$. As a consequence, one may anticipate that a (weak) paramagnetochiral dichroism (XMχD) might be found. Baranova and Zel'dovich [53] and others [54, 55] predicted long time ago that such a dichroism should be detectable at optical wavelengths, where the contribution of the $E1M1$ interference terms is dominant; but the theory of optical magnetochiral dichroism (OMχD) is more complicated because the Zeeman effect and the contribution of the spin anapole must also be taken into account. The first OMχD spectra were reported rather recently in solutions of paramagnetic chiral compounds [56, 57] and even in diamagnetic systems [58, 59]. Nevertheless, no XMχD could unfortunately be detected as yet on chiral paramagnetic solutions. On the other hand, the problem of detecting XMχD spectra using powdered samples of magnetic chiral complexes is different because the orientations of the cristallites are frozen and another way to define the quantization axis must be found. In this case, it is desirable to combine the electric and magnetic fields in a geometry depending on the magnetic group of the sample. Further work is in progress at the ESRF in order to explore this possibility, which is reminiscent of the induced magnetoelectric effect detected in the paramagnetic phase of $NiSO_4{\cdot}4H_2O$ [60].

For completeness, we have also listed the effective

operators related to the parity-even EEH susceptibilities in column 2 of Table 4. These operators can be seen as describing the magnetoelectric properties induced by the electric field. The first term is a free energy violating the time-reversal symmetry. It should be kept in mind that the corresponding systems having even parity are strictly speaking not relevant to optical activity any more. In the X-ray range, they could nevertheless contribute to the σ_{E2E2} or σ_{E1E3} absorption cross sections, which are unfortunately significantly smaller than σ_{E1E2}.

3.2. Natural X-ray optical activity

According to [27], the effective operator

$$\mathbf{N}^{(2,+1)} = [\mathbf{L}, \mathbf{\Omega}]^{(2)}$$

associated with natural XOA is the Θ-even direct product of two Θ-odd operators that are both related to orbital magnetism. This suggests viewing the natural XOA either as a «degenerate» case of orbital magnetism or as a particular case of the «induced orbital magnetoelectric effect». We also note that $\langle \mathbf{N}^{(2,+1)} \rangle$ may well be nonzero even when either $\langle \mathbf{L} \rangle$ or $\langle \mathbf{\Omega}^{(1,-1)} \rangle$ is zero. This can easily be illustrated with the case of diamagnetic chiral compounds: Lloyd's theorem implies that $\langle \mathbf{\Omega}^{(1,-1)} \rangle$ must vanish, whereas $\left\langle [\mathbf{L}, \mathbf{\Omega}]^{(2,+1)} \right\rangle$, which is Hermitian but Θ-even, can perfectly remain finite.

There is another case that deserves a special attention: if the expectation value of the orbital anapole moment is nonzero along the direction of the wave vector $\mathbf{k}$, then the system must exhibit a magnetochiral dichroism (XMχD) in addition to the natural circular dichroism (XNCD). Moreover, one would expect the external magnetic field not only to create a magnetization vector $\mathbf{M}$, but also to stabilize one isomer with respect to its enantiomer as a consequence of the parity-violating free energy $[\mathbf{\Omega} \cdot \mathbf{M}]$; this effect has been proved experimentally using OMχD [57]. This experiment may shed new light on a long-lasting debate regarding the existence of chirality in prebiotic chemistry [61–63], because it suggests that the action of a strong magnetic field can suffice to resolve optical enantiomers. This would revivify the old view of Pasteur [64] that an intrinsic dissymmetric force is inherent to the physical world. We recall that Pasteur, with his remarkable intuition, tried hard for many years to show that chirality and magnetism are connected [64], but he could not prove this within the knowledge of his time.

As already illustrated with the first column of Table 4, the dyad $[\mathbf{L}, \mathbf{\Omega}]$ can be decomposed into three irreducible representations: the pseudoscalar

$$\mathbf{N}^{(0)} = [\mathbf{L}, \mathbf{\Omega}]^{0},$$

the dual polar vector

$$\mathbf{N}^{(1)} = [\mathbf{L} \times \mathbf{\Omega} - \mathbf{\Omega} \times \mathbf{L}]^{(1)},$$

and the pseudodeviator $\mathbf{N}^{(2)}$, which was shown to play a key role in XOA. *A priori*, the scalar part $\mathbf{N}^{(0)}$ could only be associated with the $E1M1$ interference terms that dominate optical activity at optical wavelengths but can be neglected in the X-ray range as proved in the next subsection. One may wonder, however, whether any specific XOA effect may be related to the vector term $\mathbf{N}^{(1)}$. An interesting indication can be found in the early works [65] and [66], where it was suggested that a new type of optical activity can be measured in the reflectivity mode for several crystal classes. More recently [67], it was pointed out that these mysterious classes are precisely associated with the irreducible vector part of the optical activity tensor. In Table 5, following [67], we have listed the crystal classes that can contribute to a scalar, vector or tensor type XOA according to symmetry. But we must identify where the theory developed in Subsec. 2.2 is to be modified in order to become compatible with the eventual detection of the vector part of natural optical activity in the X-ray regime. The solution to this puzzling problem was more or less given in [68], where it was pointed out that in all crystal classes exhibiting the vector optical activity, the electromagnetic wave propagating inside the crystal is not transversally polarized but has a so-called skew polarization with an axial component. It has to be realized, however, that the absorption cross section σ_{E1E2} of such a very weak axial component is a second-order dichroism, whose detection would be a considerable challenge for experimentalists. Recently, we nevertheless succeeded in detecting the vector type of natural optical activity of a diamagnetic zinc oxide (ZnO) single crystal, in a geometry optimized for X-ray resonant scattering [69].

Induced natural optical activity can also be predicted to occur as a consequence of the $m = 4$ terms in Eq. (14). The two rank-3 operators

$$\mathbf{\Gamma}^{(3,-1)} = \left[[\mathbf{L}, \mathbf{L}]^{2}, \mathbf{\Omega}\right]^{(3,-1)},$$

$$\mathbf{\Delta}^{(3,+1)} = \left[[\mathbf{n}, \mathbf{L}]^{2}, \mathbf{\Omega}\right]^{(3,+1)}$$

can induce natural optical activity. We have already emphasized that $\mathbf{\Gamma}^{(3,-1)}$ is odd with respect to I and Θ,

Table 5. Rotational invariants of natural optical activity

Natural OA	Irreducible parts of $\mathbf{L} \otimes \mathbf{\Omega}$		
Crystal classes	Pseudoscalar	Polar vector	Pseudodeviator
1; 2; 3; 4; 6	1	1	1
622; 32; 422; 222	1	0	1
m; $mm2$	0	1	1
$\bar{4}$; $\bar{4}2m$	0	0	1
$6mm$; $3m$; $4mm$	0	1	0
432; 23	1	0	0

whereas $\mathbf{\Delta}^{(3,+1)}$ is even with respect to both I and Θ. Typically, $\Delta^{(3,+1)}$ originates in the $m = 4$ biquadratic magnetoelectric susceptibility and appears as the operator responsible for electrogyration in centrosymmetric solids, under high magnetic fields, $\mathbf{\Gamma}^{(3,-1)}$ can induce XNCD signals in noncentrosymmetric magnetic systems, possibly in powdered samples. It seems that the latter operator could be responsible for the so-called quadratic Faraday effect of optically active systems. We recall that there are magnetic groups that are not magnetoelectric but nevertheless admit $\mathbf{\Gamma}^{(3,-1)}$ as irreducible representations. Nevertheless, the $m = 4$ terms in Eq. (14) are expected to be rather small; as yet, we failed to prove that electrogyration can be measured in the X-ray spectral range.

3.3. Rotational isotropy

3.3.1. XNCD spectra

It was obvious from the beginning that the X-ray natural circular dichroism (XNCD) can hardly be detectable in powders or solutions because the rank-3 tensor $E1E2$ has no scalar part. This is not surprising because the spherical harmonics associated with the electric dipole ($\ell = 1$) and electric quadrupole ($\ell = 2$) are orthogonal in a sample that is orientationally isotropic. For the sake of illustration, we have reproduced in Fig. 2*a* the cobalt K-edge X-ray absorption near edge (XANES) and XNCD spectra of two resolved enantiomers of the chiral «propeller-like» complex

$$\mathbf{1}^{\pm} = 2[\mathrm{Co(en)_3Cl_3}] \cdot \mathrm{NaCl} \cdot 6\mathrm{H_2O}.$$

In these compounds, the ligand field has the D_3 point group symmetry. As already reported elsewhere [18],

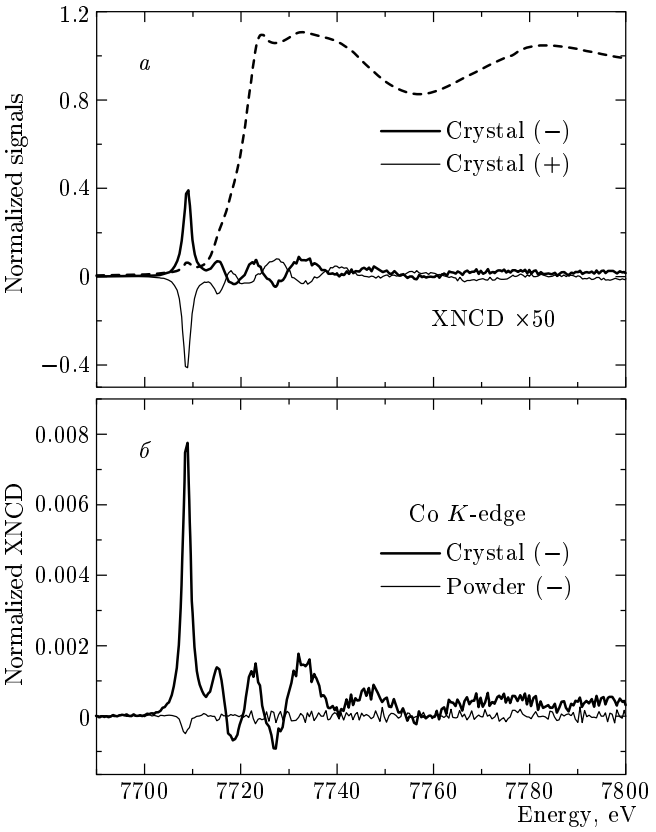

Fig. 2. Co K-edge XNCD spectra of the resolved enantiomers of the chiral complex $\mathbf{1}^{\pm} = 2[\mathrm{Co^*(en)_3Cl_3}] \cdot \mathrm{NaCl} \cdot 6\mathrm{H_2O}$. *a* — XNCD spectra recorded with single crystals of the (+) and (−) enantiomers. A polarization-averaged XANES spectrum was added for comparison. *b* — XNCD spectra of the (−) enantiomer as a single crystal or as a powdered pellet. Note the very weak, inverted signal obtained with the powdered pellet

the XNCD spectra of the two enantiomers have opposite signs. In Fig. 2*b*, we compare the XNCD spectra recorded with either a single crystal or a pellet of a powdered sample of the same enantiomer. With the powdered sample, the strong XNCD signature assigned to the $E1E2$ interference terms totally vanishes. However, a very weak signal that has the opposite sign is left in the preedge range (the normalized amplitude is approximately $2.5 \cdot 10^{-4}$). It is impossible to transform the XNCD spectrum of a given enantiomer into the spectrum of its mirror image by a simple rotation. This implies that the very weak signal observed in the powdered sample cannot be explained by any residual orientational order in the powder. It is therefore our interpretation that this weak signal should be of a different nature and can be associated with small $E1M1$ pseudoscalar interference terms.

Regarding the photoexcitation of deep core states, a monoelectronic $M1M1$ transition is forbidden for two independent reasons: (i) the angular momentum operator $\mathbf{L}$ has zero eigenvalue for a spherically symmetric $1s$ core state (e.g., in the case of a K-edge photoionization); (ii) in a central-field atomic model, one-electron radial wave functions with the same ℓ and different energies are orthogonal, and the magnetic dipole transition matrix element therefore vanishes. In a many-body picture, the second argument no longer applies because different potentials must be used to describe initial and final one-electron states [13], but argument (i) is still a problem. It is our interpretation that $E1M1$ transitions can nevertheless be allowed in the case of a multielectron excitation process. This interpretation is supported by the derivation [37] of a two-particle $E1M1$ sum rule via the same procedure as that described in Sec. 2.3. The calculated effective operator was identified as a two-particle orbital pseudoscalar $\mathbf{N}^{(0)} = \mathbf{L} \cdot \mathbf{\Omega}$. Typically, one X-ray photon would cause the simultaneous photoexcitation of two electrons, one in the deep K-shell and the other in the valence band. That the effective operator vanishes ($\mathbf{N}^{(0)} \equiv 0$) for a single particle follows from the definition

$$\mathbf{N}^{(0)} = \mathbf{L} \cdot [(\mathbf{L} \times \mathbf{n}) - (\mathbf{n} \times \mathbf{L})]/2.$$

The experimental and theoretical results thus suggest that (difficult) XNCD experiments on powdered samples could possibly give access to the effective operators of parity-mixing many-body processes, of which very little is presently known.

When no single crystal is available, there is still a possibility to recover a well detectable XNCD_{E1E2} signal: the idea is to break the orientational isotropy of space artificially, e.g., by investigating liquid crystal phases aligned in a high magnetic field or chiral ferromagnets below their Curie temperature [70]. As an example, we report the XNCD spectra of another stereogenic organometallic complex,

$$\mathbf{2}^{\pm} = [(\mathrm{L}_1)(\mathrm{L}_2)\mathrm{Fe}^{II}(\mathrm{L}_3)(\mathrm{L}_4)],$$

dissolved in an aligned liquid crystal. In this tetracoordinated iron complex, the absorbing atom (Fe) is clearly in a chiral ligand field because all the four ligands are different (the point group C_1): L_1 is the cyclopentadienyl ligand ($\eta^5 - \mathrm{C}_5\mathrm{H}_5$), L_2 is a iodine atom ($-\mathrm{I}$), L_3 is a carbonyl group ($-\mathrm{CO}$), and L_4 a chiral tertiary phosphine ($-\mathrm{PPh}_2\mathrm{R}$) with R = ($-$NMe-C*HMePh). The stereoselective synthesis of the corresponding diastereo-isomers was first described in [71] and was reproduced for us at the University of Dijon (France). Because no large-size single crystals could be grown, the enantiomers were dissolved in a liquid crystal that was known to exhibit a strong diamagnetic anisotropy (Merck: MLC-6204 ; $T_c = 66^{\circ}C$) and each chiral sample was aligned in a 5 T magnetic field directed along the wave vector $\mathbf{k}$ of the incident X-ray beam. We recall that the exploitation of mesophase-oriented solutes has become a very popular technique in NMR and ESR since the pioneering work of Saupe in 1963 [72, 73]. In Fig. 3, we have reproduced the Fe K-edge XANES and XNCD spectra of the two enantiomeric solutions. The two XNCD spectra have clearly opposite signs, as expected. The price that we had to pay was clearly a dramatic loss of sensitivity, not only because the solubility of the chiral complexes was very poor, but also because the (unknown) order parameter of the solute itself inside the liquid crystal phase was probably rather low. We note that *ab initio* simulations of the experimental XNCD spectra turned out to be impossible unfortunately due to the lack of information regarding the preferential orientational order of the solute in the oriented liquid crystal.

3.3.2. Nonreciprocal XMχD and XMLD spectra

Magnetochiral dichroism (XMχD) spectra of $\mathrm{Cr}_2\mathrm{O}_3$ were successively recorded using either a single crystal or a powdered sample [14]. As illustrated by Fig. 4, the most significant difference between the two spectra is a reduction of the signal, approximately 6 : 1 in the experiment carried out with the powdered sample. It also appears that the normalized intensity of the magnetochiral dichroism spectrum measured with the single crystal exceeds the intensity of the XNCD spectra reproduced in Fig. 2; this might well be consistent

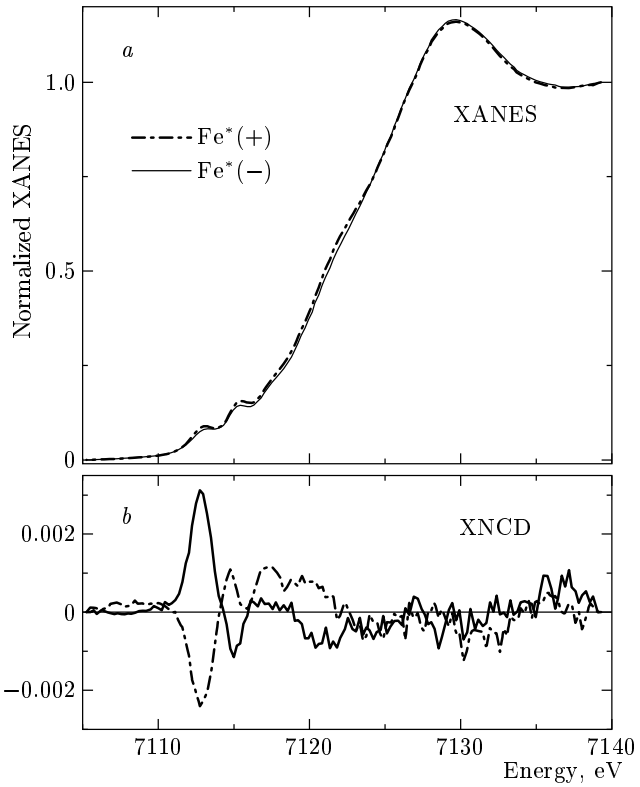

Fig. 3. Fe K-edge XNCD spectra of the two resolved enantiomers of the chiral complex $\mathbf{2}^{\pm}$ = $(\eta^5 - C_5H_5)Fe^*(-I)(-CO)[-PPh_2(-NMe - C^*HMePh)]$ dissolved in a liquid crystal phase (Merck ZLI 4814). All spectra were recorded in the fluorescence detection mode using a high magnetic field (5 T) to align the liquid crystal and the solute. a — Polarization averaged XANES spectra of each (±) enantiomer. b — XNCD spectra of the two (±) enantiomers

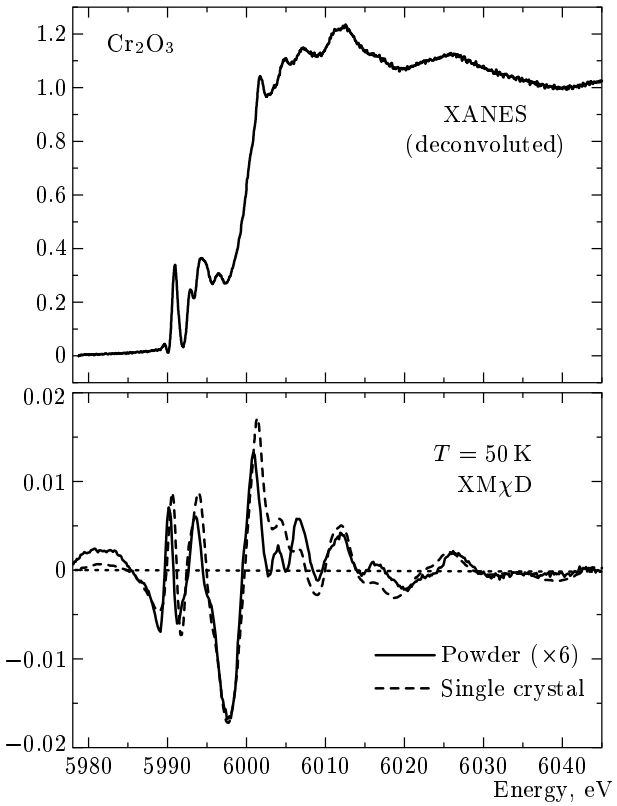

Fig. 4. Cr K-edge XMχD spectra of Cr_2O_3 recorded with either a single crystal ($\mathbf{c}\|\mathbf{k}$) or a powdered sample. The differential absorption spectra refer to the 180° domains grown under the condition of time-reversality after magnetoelectric annealing. The upper trace reproduces a high energy resolution (deconvoluted) XANES spectrum

with our remark that the magnetoelectric susceptibilities $[a_{\alpha\beta}]_{orb}$ appear in the lowest order term $m = 2$ of the series expansion of the energy $U(\mathbf{L}, \mathbf{n})$, whereas the effective operators for XNCD contribute to the $m = 3$ susceptibilities.

The primary aim of this section is to show that the proved capability to record XMχD spectra using powdered samples is fully consistent with the proposed sum rule analysis and also consistent with our interpretation that the leading term in Eq. (3) should be the contribution of the projection of the orbital anapole moment $\mathbf{\Omega}_0^{(1)}$ along the direction of the wave vector $\mathbf{k}$. Since the pioneering works of Astrov [74, 75], it is well documented that the key step in measurement of the magnetoelectric susceptibility is the creation of a remanent state characterized by a strong polarization of the magnetoelectric domains. This is rather well understood for Cr_2O_3, which has only two magnetoelectric domains (±) that can be exchanged by reversing the time and are illustrated with Fig. 5. If $n_{(+)}$ and $n_{(-)}$ denote the number densities of the two types of domains, we are directly concerned in our experiment with the magnetoelectric polarization ratio

$$\rho_{ME} = \frac{n_{(+)} - n_{(-)}}{n_{(+)} + n_{(-)}}.$$

We found it most convenient to adapt the model proposed in [76] to describe the nucleation of magnetoelectric domains by annealing.

We start from a crystal that is described by the tensors $\langle \mathbf{T}_\beta^{(b,\theta)} \rangle_X$ in the crystalline axes. In a powder, the crystalline axes of a given crystallite i are rotated with respect to the reference frame of the experiment, with the rotation described by the Euler angles ϕ_i, θ_i, and ψ_i. We assume that the electric and magnetic fields

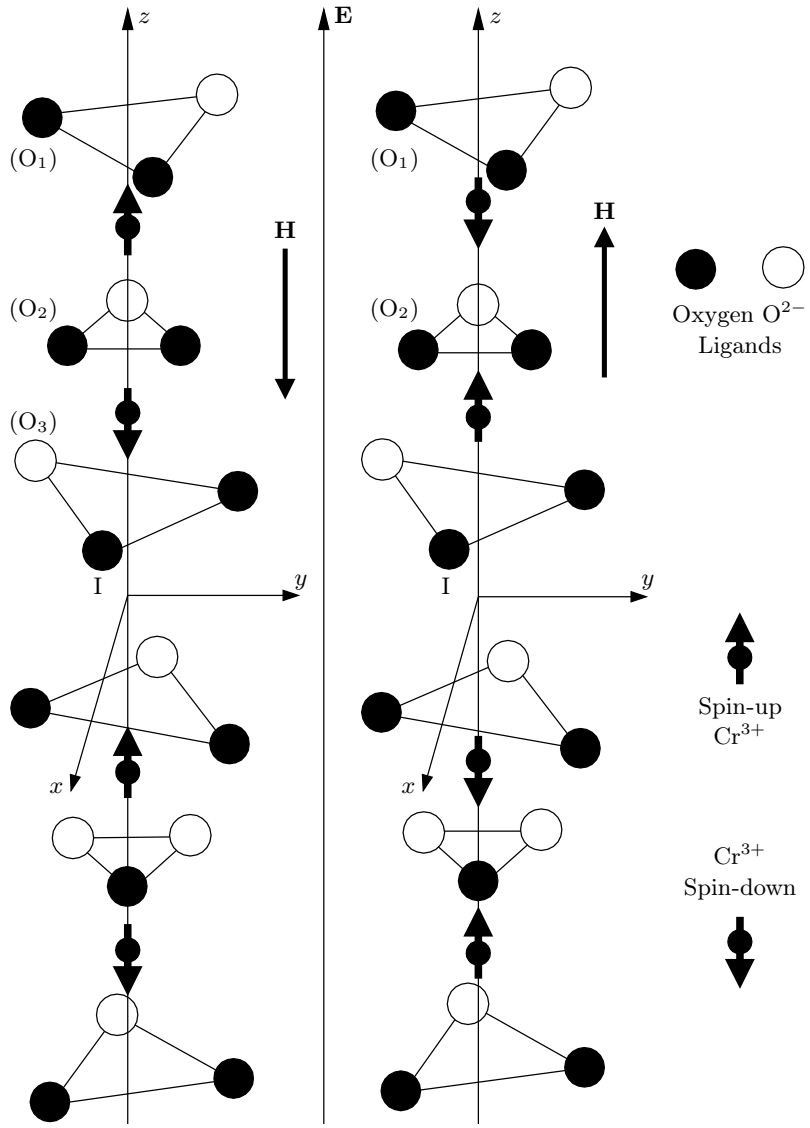

Fig. 5. Schematic representation of the two 180° antiferromagnetic domains grown by magnetoelectric annealing with antiparallel (left panel) and parallel (right panel) electric (**E**) and magnetic (**H**) fields

are parallel to the z axis of the reference frame of the experiment and that the magnetoelectric tensor of the crystal is diagonal (with $\alpha_{xx} = \alpha_{yy}$) in the reference frame of the crystal. The magnetocrystalline energy of the crystallite is therefore proportional to (see [77])

$$U_{ME}(\theta_i) = -\mathbf{E}\cdot\alpha\cdot\mathbf{H} = -EH(\alpha_{zz}\cos^2\theta_i + \alpha_{xx}\sin^2\theta_i)$$

for a domain of the magnetoelectric type and to $-U_{ME}(\theta_i)$ for domains of other types. At the temperature T_N, the polarization ratio is given by

$$\frac{n_{(+)} - n_{(-)}}{n_{(+)} + n_{(-)}} = \rho_{ME}(\theta_i) = \mathrm{th}\left(\frac{U_{ME}(\theta_i)}{kT_N}\right). \qquad (15)$$

The XOA experiments refer to tensors $\langle \mathbf{T}_\beta^{(b,\theta)}\rangle_X$ that not only are parity-odd but also change sign for domains of different types. For a crystallite i, the tensors in the reference frame of the experiment become

$$\sum_{\beta'} \mathbf{D}^{(b)}_{\beta'\beta}(\phi_i,\theta_i,\psi_i)\langle \mathbf{T}_\beta^{(b,\theta)}\rangle_X \tanh(U_{ME}(\theta_i)/kT_N).$$

To obtain the tensor components $\langle \mathbf{T}_\beta^{(b,\theta)}\rangle_p$ of the powder, we calculate the average of the last expression over ϕ_i, θ_i, and ψ_i. The average over ϕ_i and ψ_i gives $\beta' = 0$ and $\beta = 0$. From

$$\mathbf{D}^{(b)}_{00}(\phi_i,\theta_i,\psi_i) = P_b(\cos\theta_i)$$

(where P_b is a Legendre polynomial), we find that

$$\langle \mathbf{T}_\beta^{(b,\theta)} \rangle_p = \delta_{\beta,0} \langle \mathbf{T}_0^{(b,\theta)} \rangle_X I_b,$$

where

$$I_b = \int_0^1 P_b(x) \operatorname{th}\left\{\alpha\left[\left(1+\beta^2\right)x^2 - \beta^2\right]\right\} dx,$$

with

$$\beta^2 = -\frac{a_{xx}}{a_{zz}} \ll 1, \quad \alpha = -\frac{EH\alpha_{zz}}{kT_N}.$$

We note that the integral is restricted to the range 0 to 1 by symmetry. In this context, the macroscopic magnetoelectric susceptibility $J_2 = (2I_2 + I_0)/3$ measured with a powdered sample must be given by [76]

$$J_2 = \int_0^1 x^2 \operatorname{th}\left\{\alpha\left[\left(1+\beta^2\right)x^2 - \beta^2\right]\right\} dx.$$

In Table 6, we have regrouped the calculated values of the integrals I_b (≤ 3) for typical values of the parameters α and β^2. Because the efficiency of the magnetoelectric annealing procedure carried out with the single crystal is not known, the values listed in Table 6 are systematically normalized with a constant scaling factor slightly less than unity, $\operatorname{th}\alpha_0 \approx 0.995$ if $\alpha_0 = 3$. Following [76], we have assumed in the first two examples that at least near the Néel temperature T_N, $\beta^2 \approx 0$, and we compared the integrals obtained with $\alpha_0 = 3$ and $\alpha = 1$. In the last simulation, which seems to be a reasonable approximation of our experimental conditions, we selected $\alpha = 1$ and $\beta^2 = 0.15$. In all cases, I_3 is quite small (≤ 0.05); it even reverses its sign when the magnetoelectric polarization of a well-oriented crystallite is assumed to be as effective as in the case of a single crystal ($\alpha_0 = 3$). We also note that the experimental value $J_2 \approx 0.3$ reported in [75] is very close to the asymptotic value that should be measured when the annealing process is as effective in the powder as in the single crystal. In practice, unless very careful annealing procedures are used (e.g., heating the powder at 1300°C under inert atmosphere), the local electric field in the powder can be dramatically reduced due to the hygroscopic character of the powder, while the conductivity increases, as pointed out in [77]. As a result, we expect a certainly lower efficiency of our annealing, as reflected by $\operatorname{th}\alpha \approx 0.76$ for $\alpha = 1$.

An important result of this calculation is that $\left\langle \mathbf{\Gamma}_0^{(3,-1)} \right\rangle$ should have only a very small contribution in the powdered sample; because the two XMχD spectra displayed in Fig. 4 exhibit only minor differences, we are therefore led to the important conclusion that the application of the sum rule to the XMχD spectrum recorded with the single crystal should yield a reasonable estimate of the orbital anapole moment.

A further question is whether nonreciprocal XMLD spectra can also be recorded using powdered samples. The answer strongly depends on how the magnetoelectric annealing procedure is conducted. We can assume, for instance, that the same type of annealing is again performed with a powdered sample of Cr_2O_3, but in the different geometry, $\mathbf{E} \parallel \mathbf{H} \perp \mathbf{k}$. In other terms, we have set a different direction of quantification for the magnetoelectric domains in the laboratory coordinates $\{X, Y, Z\}$, whereas the free energy in the cristallite coordinates $\{x, y, z\}$ remains unchanged. Hence,

$$\left\langle W_{XX}^{(2,-1)} \right\rangle - \left\langle W_{YY}^{(2,-1)} \right\rangle \propto$$
$$\propto \int_0^1 \left[\left(a_{zz} - a_{xx}\right)x^2 + a_{xx}\right]_{orb} \times$$
$$\times \operatorname{th}\{\alpha\left[\left(1+\beta^2\right)x^2 - \beta^2\right]\} dx.$$

We thus expect a nonreciprocal XMLD (S_2) signal to be measurable in the powdered sample: it should now be proportional to J_2, under the assumption that

$$\left(a_{zz} - a_{xx}\right)_{orb} \neq 0.$$

It would be interesting to compare such a nonreciprocal XMLD spectrum with a test experiment carried out with a single crystal in a geometry satisfying the condition $\mathbf{c} \perp \mathbf{k}$, with the magnetoelectric annealing still performed with $\mathbf{E} \parallel \mathbf{H} \parallel \mathbf{c}$. A comparison of this type would yield valuable information regarding the importance of the septor term in XMLD experiments.

In powdered samples, as suggested in [78], annealing could be carried out in electric and magnetic fields arbitrarily oriented with respect to each other. In the cristallite coordinates $\{x, y, z\}$, the relevant magnetoelectric free energy must be replaced by

$$U_{ME} \propto -EH[\left(a_{zz}\cos^2\theta_i + a_{xx}\sin^2\theta_i\right)\cos\beta_0 +$$
$$+ \left(a_{zz} - a_{xx}\right)\sin\theta_i\cos\theta_i\sin\phi_i\sin\beta_0].$$

Because the term proportional to $\sin\phi_i$ has zero average in the calculation of the modified integral J_2, we can anticipate that the price to be paid is a further reduction of the annealing efficiency proportional to $\cos\beta_0$, where β_0 denotes the angle between the electric and magnetic fields. This result was not really unexpected. It is, however, restricted to magnetoelectric solids that have a diagonal magnetoelectric tensor with $a_\parallel \gg -a_\perp$. We will consider the general

Table 6. Rotational average integrals for powdered samples

Parameters	I_0	I_1	I_2	I_3	J_2
$\alpha_0 = 3.0$, $\alpha = 3.0$, $\beta^2 = 0.0$	0.565	0.387	0.150	−0.008	0.289
$\alpha_0 = 3.0$, $\alpha = 1.0$, $\beta^2 = 0.0$	0.296	0.218	0.109	0.026	0.172
$\alpha_0 = 3.0$, $\alpha = 1.0$, $\beta^2 = 0.15$	0.202	0.184	0.131	0.051	0.155

case of the magnetoelectric annealing of powdered samples depending on the magnetoelectric symmetry of the cristallites elsewhere [79].

4. APPLICATIONS OF X-RAY OPTICAL ACTIVITY

4.1. Magnetoelectric symmetry

4.1.1. Chromium sesquioxide: Cr_2O_3

The detection of rather intense XMχD spectra in the magnetoelectric phase of Cr_2O_3 (eskolaite) is somewhat puzzling because the universally cited magnetic group of Cr_2O_3, i.e., $\bar{3}'m'$, does not admit the anapole as an irreducible representation, $\mathbf{\Omega}_0^{(1)} = 0$. According to Table 3, the septor $\mathbf{\Gamma}_\beta^{(3,-1)}$ must have only a single nonzero component, but the table itself does not tell us whether this component is for $\beta = 0$. This is precisely where the method developed in Sec. 2.3 can help us. For the magnetic group $\bar{3}'m'$, we obtain that

$$\langle \mathbf{T}_\beta^{(1,-1)} \rangle = 0,$$
$$\langle \mathbf{T}_\beta^{(2,+1)} \rangle = 0,$$
$$\langle \mathbf{T}_\beta^{(2,-1)} \rangle = \delta_{\beta,0} \mathbf{T}_0^{(2,-1)},$$
$$\langle \mathbf{T}_3^{(3,-1)} \rangle = \langle \mathbf{T}_{-3}^{(3,-1)} \rangle = \frac{\mathbf{T}_3^{(3,-1)} + \mathbf{T}_{-3}^{(3,-1)}}{2}.$$

The other components of $\mathbf{T}^{(3,-1)}$ are zero, including the one for $\beta = 0$. Morever, we note that when the wave vector is directed along the z axis of the reference frame (which is also the **c** axis of the crystal), then $\mathbf{T}_{\pm 3}^{(3,-1)} = 0$. In other terms, $\mathbf{T}^{(3,-1)}$ cannot be detected in this geometry. In conclusion, there is no optical activity of any type compatible with the group $\bar{3}'m'$, in the geometry of the experiment.

It must also be kept in mind that whatever the true magnetic group of Cr_2O_3 may ultimately be, a component $\Gamma_0^{(3,-1)}$, if any, should give only a very weak contribution to the spectrum recorded in the powdered sample. It was argued in the previous section that the spectrum recorded with the single crystal should yield a reasonable estimate of some orbital anapole moment. In all cases, this would imply a reduction of the magnetic symmetry in what we have previously called a pseudoground state. At this stage, we are left with interpretations of two types, which we now consider successively.

1. The observed reduction of the ground state magnetic symmetry of Cr_2O_3 is related to experimental conditions favoring some metamagnetic phase.

Some ambiguity may possibly stem from the fact that the XMχD spectra were recorded in the presence of a rather modest magnetic field (0.5 T) directed along the **c** axis. We recall that this magnetic field was required only to grow single antiferromagnetic domains, no magnetic field being *a priori* needed to record the XMχD spectra. It has been argued that the axial magnetic field can modify magnetic symmetry of the sample and that metamagnetic domains of symmetry $3m'$ can (eventually) contaminate the measurements. This is, however, contradicted by the fact that the sample did not exhibit any measurable XMCD spectrum at the Cr K-edge. Moreover, a quick inspection of Table 3 immediately shows that the group $3m'$ again admits only the septor but not the anapole as irreducible representations.

It has been known for decades that the magnetic group of Cr_2O_3 changes beyond the critical spin-flop transition [80, 81]. Recent investigations initiated in [82–84] have confirmed that when a strong magnetic field (up to 20 T) is applied along the **c** axis, a toroidal order can be detected that is associated with the spin-flop magnetic group $2'/m$. Because the critical spin-flop field at 100 K is 5.8 T [85], it is very unlikely that spin-flop domains could develop in a field of 0.5 T. Recent crystal topography experiments carried out with the powerful method of polarized second harmonic generation have proved that no spin-flop domain can be detected below the critical spin-flop field [85].

There are further experimental data that also concur to rule out any contribution of spin-flop domains. Unpublished X-ray linear dichroism spectra, e.g., XLD (S_1) spectra, were recorded in the presence of a higher

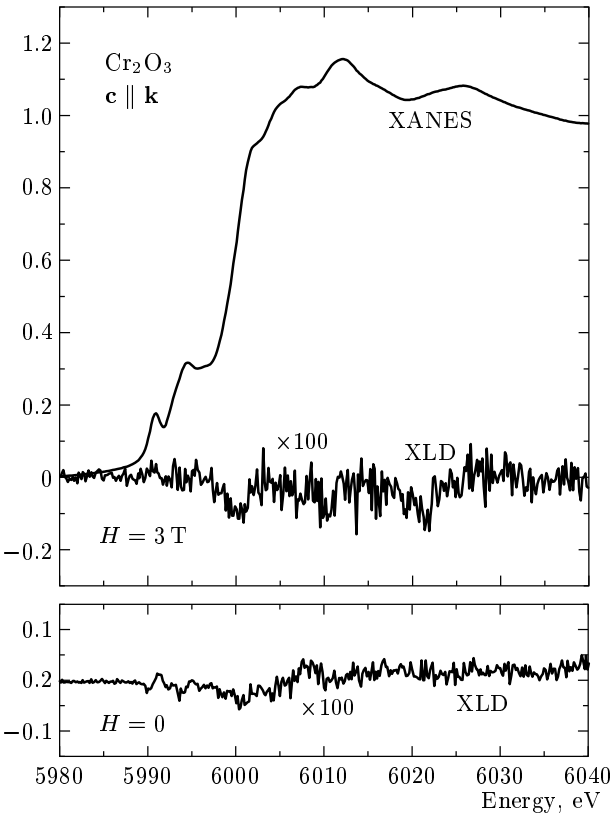

Fig. 6. Cr K-edge XLD spectra of Cr_2O_3 with or without magnetoelectric annealing using a 3 T magnetic field. The crystal and the geometry of the experiment were the same as for recording XMχD spectra ($\mathbf{c}\|\mathbf{k}$). The upper trace reproduces a XANES spectrum (raw data) for comparison

magnetic field (3 T) following a magnetoelectric annealing procedure carried out with a strong electric field (1kV/cm) in the geometry $\mathbf{E}\|\mathbf{H}\|\mathbf{c}\|\mathbf{k}$. Under such experimental conditions, one would expect the hypothetical spin-flop domains to have a stronger weight, with the practical consequence that reciprocal/nonreciprocal XLD signals should become detectable. As illustrated in Fig. 6, we found no conclusive evidence of such a dichroism. For comparison, we have included in Fig. 6 a natural XLD spectrum recorded in the absence of any magnetic field: the goal was to check carefully whether the (possibly) imperfect alignment of the **c** axis with the wave vector **k** can generate any artefactual dichroism. This is clearly not the case. These negative experiments support our view that it is very unlikely that spin-flop domains can contribute to the XMχD experiment performed with a much weaker magnetic field (0.5T). It is also noteworthy that all diagonal terms of the magnetoelectric tensor are expected to vanish in the $2'/m$ spin-flop phase [50]: no effective magnetoelectric annealing can then occur in the geometry of our XMχD experiment and the separation of domains of opposite time-reversality becomes impossible.

2. There is a reduction of the magnetic symmetry due to some partially unquenched angular momentum that has a different quantization axis than the spins.

There is nothing sacrilegious to envisage that the orbital part of the magnetoelectric tensor $[a_{\alpha\beta}]_{orb}$ (which has never been measured so far) can reveal a symmetry reduction with respect to the point group $\overline{3}m\otimes\Theta$, which admits $\overline{3}'m'$ as a subgroup. We recall that this subgroup corresponds to the highest magnetic symmetry compatible with the chemical cell (measured above T_N) and with the antiferromagnetic spin configuration. As pointed out in [86], the angular momentum unquenched by covalent bonding, with a different quantization axis than the spins, must be a widespread phenomenon in antiferromagnetic solids.

In our case, there can be no anapole component $\mathbf{\Omega}_0$ along the **c** axis without a (small) orbital moment **L** and an orthogonal electric dipole in directions perpendicular to **c** at the Cr sites. We can therefore expect a (small) canting of the total magnetic moment. We here reopen a fairly old debate that started when Foner [87] reported that the parallel magnetic susceptibility of Cr_2O_3 does not drop to zero below 4 K. This led to active search for a canted structure of the magnetic moments until Silverstein and Jacobs found that Van Vleck susceptibility calculations can explain the residual contribution of $\chi_\parallel$ [88]. We recall that the Van Vleck susceptibility accounts for localized orbital moments consistent with a Zeeman perturbation restricted to the first and second order,

$$\chi^{ii}_{orb} = \frac{N\mu_B^2}{3kT}\{\langle\Psi_g|\,L_i\,|\Psi_g\rangle\,\langle\Psi_g|\,L_i\,|\Psi_g\rangle\} + \\ + \frac{2N\mu_B^2}{3}\sum_{n\neq g}\frac{\langle\Psi_g|\,L_i\,|\Psi_n\rangle\,\langle\Psi_n|\,L_i\,|\Psi_g\rangle}{E_n - E_g}, \quad (16)$$

where N is the Avogadro number. In the particular case where the ground state is orbitally nondegenerate, the first term vanishes. This was assumed by Silverstein and Jacobs, who considered a Cr ion in a cubic crystal field with a weak trigonal field. The Van Vleck susceptibility can then only result from the temperature-independent second term, which couples the ground state to higher crystal field levels. Parallel susceptibility measurements refer to the component L_z, but the weak trigonal field splitting of the corundum structure yields an even higher coupling for $L_{x,y}$ resulting in

stronger Van Vleck contributions to $\chi_\perp$ [89]. The angular momentum alone cannot yield the orbital anapole moment; we also need electric dipoles. Recently, Muto et al. [90] tried to simulate magnetoelectric spectra at optical wavelengths and pointed out that an antisymmetric twist field with trigonal symmetry must be introduced in the microscopic model in order to mix odd-parity orbitals in the stationary states of the system. This antisymmetric twist is clearly essential to produce a nonzero local orbital anapole moment. At this stage, it is tempting to conclude that the symmetry reduction is caused by a substantial admixture of low-lying crystal field levels in the virtual ground state. We do not even require an external field to induce the Zeeman second-order perturbation; the strong exchange field responsible for the antiferromagnetic order and the spin–orbit coupling could play the same role. We recall that the strong local perturbation caused by the deep core hole can obviously also cause such a substantial coupling as predicted in Sec. 2.1 (see Eq. (3)).

It remains to be proved experimentally, however, that there is no unquenched angular momentum in the ground state of Cr_2O_3; one should also reinvestigate whether some small ordered canting of the magnetic moments associated with angular momentum can occur. Careful neutron diffraction studies [91] failed to detect any large, ordered canting of the magnetic moments, but the authors admitted openly that neutron diffraction cannot disprove models with canting angles less than 3 degrees. This implies that with the measured spin moment $2.48\mu_B$ at each Cr site, orthogonal orbital moments as large as $0.13\mu_B$ may not be seen. This leaves ample space for some orbital magnetism involving only the ground state wave functions. The authors of [92] suspected that the covalent character in the Cr–O bonds might involve «a small spin transfer from the Cr ($3d$) orbitals to the O ($2p$) shell» but they noted that the transferred moment is too small to be detected by neutron diffraction. This problem was recently reconsidered in [93] via spherical neutron polarimetry, and it was confirmed that a reduction of $\langle S_z\rangle$ from $2.98\mu_B$ to $2.48\mu_B$ is definitely too large to be explained solely by the Heisenberg «zero-point deviation» (8 %) deduced from neutron inelastic scattering measurements in [92]. Using a simple model based on a covalent overlap of the metal $3d(t_{2g})$ orbitals with the oxygen $2p$ orbitals, Brown et al. [93] pointed out that the symmetry constraints preclude a net magnetization of the oxygen atoms, and the only effect of a covalent mixing is therefore to lower the measured moment $\langle S_z\rangle$ on the Cr sites; no change of the accepted $\overline{3}'m'$magnetic group is required. This is only true if the spin–orbit coupling can be neglected as discussed below.

More sophisticated unrestricted Hartree–Fock calculations [94, 95] revealed that covalency effects are particularly important in chromium sesquioxide and can explain the well-known differences in the magnetic structures of Cr_2O_3 and Fe_2O_3. Contrary to the model in [93], Dovesi et al. [94] found a large splitting between the spin-up (t_{2g}^α) and spin-down (t_{2g}^β) states and observed that the covalent electron transfer involves a substantial contribution of the Cr $3d(e_g)$ orbitals in the ground state. This result suggests that there should be a significant contribution of the first term of the orbital susceptibility χ_{orb} expressed by Eq. (16). In the general framework of band structure calculations, the orbital part of susceptibility must also include terms, such as those predicted in [96], that have the same source as the temperature-independent Van Vleck susceptibility in localized ions.

A quick inspection of our XMχD spectra convinced us that the $E1E2$ dichroic signal is most intense for mixed parity excited states that can be identified as $\{p(O) + e_g^\alpha\}$ and $\{p(O) + e_g^\beta\}$ above the Fermi level in the unrestricted Hartree–Fock calculations in [94]. As a consequence of the crystal field symmetry, there cannot be any net spin moment delocalized on the oxygen atoms. However, the calculations produce clear evidence of a local polarization of each oxygen atom: the part of the electron cloud facing Cr_1 (α) is β polarized, while that facing Cr_2 (β) is α polarized, the maximum polarization occurring along the directions of the chemical bonds. Regarding orbital moments possibly associated with the covalent bonding, one should keep in mind that the spin–orbit coupling is expected to lower the crystal field symmetry, especially in the plane perpendicular to the **c** axis. Thus, the calculation in [94] strongly suggests that a small orbital magnetic moment perpendicular to **c** can occur at every chromium site. This is also fully consistent with the observation in [86] that highly aspherical spin densities with zero spatial average are most often associated with nonzero angular momentum distributions.

Dovesi et al. [94, 95] reiterated the claim that the magnetic symmetry of the antiferromagnetic phase of Cr_2O_3 is reduced to R3c (class $3m$), which is a subgroup of R$\overline{3}c$. It is not transparent from their paper how this claim was justified. It seems that the only magnetic constraint imposed on the calculation was that the difference between the numbers of majority-spin and minority-spin electrons per unit cell $n_\alpha - n_\beta$ was set to zero, while the program was expected to retain only solutions for which two consecutive Cr atoms

have α and β-type net atomic spin densities. Indeed, the group $3m$ would ideally explain our XOA experiments:

1) the magnetic crystal class $3m$ (space group $R3c$) admits the anapole as an irreducible representation, which is consistent with the observation of the XMχD spectra;

2) the crystal class $3m$ does not admit the pseudodeviator $\mathbf{W}^{(2,-1)}$ as an irreducible representation, which is consistent with the absence of detectable XMLD (S_1, S_2) spectra [14];

3) the crystal class $3m$ admits the septor $\Gamma^{(3,-1)}$ as an irreducible representation; using the procedure described in Sec. 2.3, we were able to check that $\left\langle \mathbf{\Gamma}_0^{(3,-1)} \right\rangle \neq 0$. From the experiment carried out with the powdered sample, we expect only a small contribution of this septor term to the XMχD spectra. On the other hand, it is easy to check that $\left\langle \mathbf{\Gamma}_{\pm 2}^{(3,-1)} \right\rangle = 0$.

Unfortunately, the magnetoelectric group $3m$ is definitely incompatible with all published magnetoelectric susceptibility measurements, including the magnetoelectric annealing procedure that we used, because it is easy to verify that the generic magnetoelectric tensor of this group has no diagonal term [50].

The point raised by Dovesi et al. that a structural change could occur below T_N would be consistent with the observation reported by several authors long ago that the lattice parameters change quite significantly below T_N [97]. Unfortunately, very high quality crystal structure data are required to refine the true magnetic space group. If we trust the interpretation that our XMχD spectra imply a reduction of magnetic symmetry below T_N, then we must seek a magnetoelectric group consistent with both XOA and the well-established magnetoelectric susceptibility measurements. The only magnetic groups that can reconcile these two experiments are $\overline{3}'$ and 3: this is because their generic magnetoelectric tensors simultaneously have the same diagonal terms as the group $\overline{3}'m'$ and the same off-diagonal terms as the group $3m$ [50]. We note that only the group $\overline{3}'$ is suitable for an antiferromagnetic solid, whereas the group 3 would imply that the system is ferromagnetic, which is not the case. Similarly, a very important observation [39] is that the existence of a magnetoelectric toroidal group requires that in the high-temperature paramagnetic phase, the compound must belong to one of the 8 ordinary groups:

$$mmm, 4/mmm, \overline{3}m, \overline{6}m2, 6/mmm, m3, \overline{4}3m, m3m.$$

Therefore, as far as the corundum point group $\overline{3}m$ is concerned, the only antiferromagnetic toroidal subgroups that deserve attention are $\overline{3}'$, $3m$, and $\overline{3}'m$, which are all subgroups of $\overline{3}'m'$. We note that only $\overline{3}'$ has a magnetoelectric tensor with diagonal elements. This was the basic argument that led us to propose this group as the true magnetic group describing the spin and orbital magnetoelectric effects in Cr_2O_3 [14]. According to Table 3, the magnetic group $\overline{3}'$ must admit irreducible representations of the type $\mathbf{W}_{\beta}^{(2,-1)}$. Using Eq. (6), we find that $\mathbf{W}_{\pm 2}^{(2,-1)} = 0$ in our experimental configuration ($\mathbf{H} \parallel \mathbf{E} \parallel \mathbf{c} \parallel \mathbf{k}$). This is fully consistent with the fact that we failed to detect any nonreciprocal XMLD signal in this geometry. As discussed in Sec. 3.3.2, a nonreciprocal dichroism XMLD (S_2) might however be detected if the wave vector $\mathbf{k}$ is set perpendicular to the $\mathbf{c}$ axis, the annealing being still performed with $\mathbf{H} \parallel \mathbf{E} \parallel \mathbf{c}$. Unfortunately, no experiment has yet been performed in this geometry.

4.1.2. Vanadium sesquioxides: $(V_{1-x}Cr_x)_2O_3$

The magnetic structure of the chromium doped vanadium sesquioxides $(V_{1-x}Cr_x)_2O_3$ in the so-called antiferromagnetic «insulating» low-temperature phase is another controversial subject. It dates back to 1980 when Word et al. [98] reported a careful neutron diffraction study on pure vanadium sesquioxide (karelianite). They confirmed that in the monoclinic antiferromagnetic insulating phase, the crystal has a distorted $I2/a$ symmetry and that the vanadium atoms carry a magnetic moment approximately given by $1.2\mu_B$, tilted away from the trigonal $\mathbf{c}$ axis by 71° and perpendicular to the $\mathbf{a}$ axis. However, the observation of a forbidden reflection for $\ell = 6h + 3$ [99] led them to envisage that the magnetic group might not be $2/m \otimes \Theta$ as is usually accepted but rather a low-symmetry group 2 [98]. They tentatively explained this symmetry reduction by a small magnetic contribution of the oxygen lattice [99]. This puzzling observation was nevertheless considered a «minor issue» even though it was admittted by Moon himself [100] and by von Laar and Yethiraj [101] that a reduction of the magnetic symmetry could be perfectly envisaged. Moon explicitly mentioned in his paper that orbital moments could result in a reduction of symmetry.

The neutron diffraction study in [98] is pertinent here because the class 2 is magnetoelectric; according to Table 3, it simultaneously admits $\mathbf{\Omega}^{(1,-1)}$, $\mathbf{W}^{(2,-1)}$, and $\mathbf{\Gamma}^{(3,-1)}$ as irreducible representations, and the measurement of nonreciprocal XMLD (S_1, S_2) spectra must then be allowed by symmetry. Using a crystal of chromium doped vanadium sesquioxide, i.e., $(V_{1-x}Cr_x)_2O_3$ with $x = 0.028$, we observed in the mon-

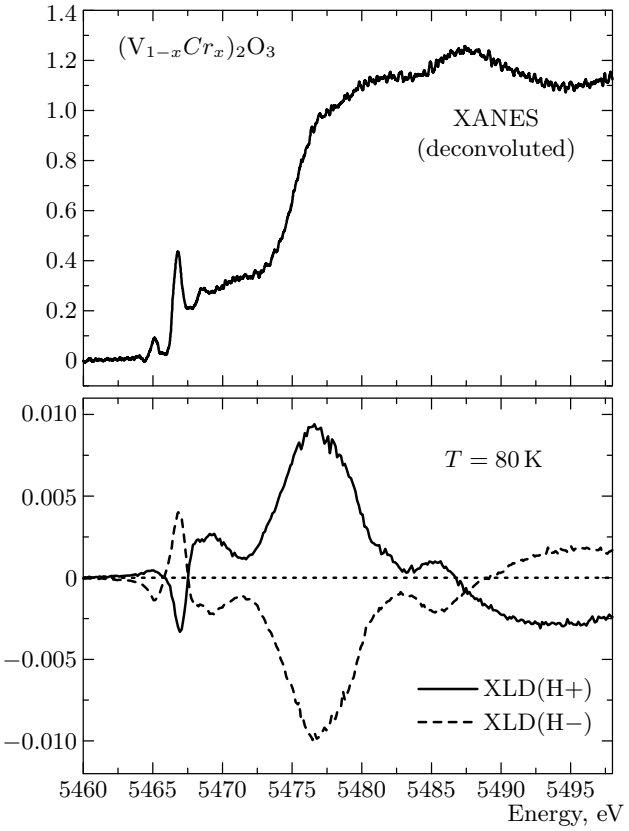

Fig. 7. V K-edge nonreciprocal XMLD spectra of $(V_{(1-x)}Cr_x)_2O_3$ recorded in the monoclinic antiferromagnetic insulating phase below T_N after magnetoelectric annealing performed with either *parallel* (+) or *antiparallel* (−) electric and magnetic fields in the geometry ($\mathbf{c}\|\mathbf{k}\|\mathbf{E}\|\mathbf{H}$). The differential absorption spectra refer to the domains grown under the condition of time-reversality after magnetoelectric annealing. The upper trace reproduces a high energy resolution (deconvoluted) XANES spectrum

oclinic low-temperature phase what is still believed to be the first example of a nonreciprocal X-ray magnetic linear dichroism [15]. The crystal borrowed from Paolasini was initially assumed to be cleaved perpendicularly to the hexagonal **c** axis, but it was realized recently that it was slightly miscut. Thus, the nonreciprocal XMLD (S_1) spectra reproduced in Fig. 7 were recorded after a magnetoelectric annealing process conducted in the geometry $\mathbf{E}\|\mathbf{H}\|\mathbf{k}$ with **c** tilted away from **k** by approximately 10°. Because the signal was found to change its sign when the annealing was performed with parallel or antiparallel electric/magnetic fields and to vanish above the Néel temperature $T_N = 181$ K, we feel that there is very little doubt left regarding the nonreciprocal character of this signal. We emphasize that the orientations of the crystallographic axes **a** and **b** were unfortunately unknown in this experiment: this makes it impossible to clarify whether the nonreciprocal dichroism that was measured is to be interpreted as the Jones dichroism XMLD (S_2) associated with the effective operator $\left[W_{bb}^{(2,-1)} - W_{aa}^{(2,-1)}\right]$ or as a true dichroism of the type XMLD (S_1) associated with the symmetric off-diagonal terms $\left[W_{ab}^{(2,-1)} + W_{ba}^{(2,-1)}\right]$. We note that we refer here to the crystal axes and not to the laboratory frame. Clearly, future experiments of this type would call for a detailed (systematic) analysis of the angular dependence of the signal with respect to 2ψ, even though one can anticipate that such experiments should be very demanding in terms of beam time allocation. Moreover, because no experiment has yet been performed with a powdered sample, no indications are available as to whether the septor terms give any significant contribution.

We note that the nonreciprocal XMLD signal measured in $(V_{1-x}Cr_x)_2O_3$ and the nonreciprocal XMχD signal of Cr_2O_3 are of approximately the same order of magnitude, the nonreciprocal XMLD signal being perhaps slightly less intense. We insist that several reasons make it impossible to interpret the spectra reproduced in Fig. 7 as classical magneto-optical (reciprocal) XMLD spectra [48]: (i) a nonreciprocal dichroism changes its sign when the magnetic field is reversed, while this is not the case for the magneto-optical XMLD spectra; (ii) in the experiment illustrated with Fig. 7, the magnetic field was oriented along the direction of the wavevector **k**, whereas the magnetic field is typically set perpendicular to **k** in magneto-optical experiments; (iii) the intensity of our nonreciprocal XMLD signal is exceeding (by one order of magnitude at least) the highest intensity that one would expect for a reciprocal, Θ-even XMLD signal. Everyone who has tried to measure a reciprocal XMLD signal at a K-edge would agree with us that this is always a very challenging experiment.

As pointed out in [15], a careful examination of the spectra reproduced in Fig. 7 reveals that there is unambiguously a weak dichroism contribution that does not change its sign when the magnetic field is reversed. Our interpretation is that this residual reciprocal signal can result either from the (small) monoclinic distortion or from the fact that the crystal was slightly miscut (or both).

As in the case of Cr_2O_3, the dichroism intensity seems to be most intense for the final states of mixed parity $3d(e_g) + O(p)$. Dovesi et al. [95] also performed unrestricted Hartree–Fock calculations on

V_2O_3, but their calculations were unfortunately conducted with the high-temperature corundum structure of V_2O_3 and still with the previous magnetic group R3*c*. It would be desirable to reproduce such calculations with the distorted monoclinic structure $I2/a$ that is widely accepted for the low-temperature antiferromagnetic phase.

In a recent theoretical study of V_2O_3, Di Matteo et al. [102] have identified two magnetoelectric subgroups of $2/m \otimes \Theta$ that can be compatible with the *X*-ray diffraction data in [103]: $2/m'$ and $2'/m$. From the tensor tables in [50], it immediately follows that the generic magnetoelectric tensor of the group $2'/m$ has no diagonal terms and cannot give any dichroism of the type XMLD (S_2). Moreover, because $[a_{cc}] = 0$, no magnetoelectric annealing is possible in our experimental configuration. In contrast, $[a_{cc}] \neq 0$ for the group $2/m'$ which looks like the ideal choice for nonreciprocal XOA experiments in our experimental configuration because this magnetic group admits the anapole as the irreducible representation along the **c** axis, while

$$\left[W_{bb}^{(2,-1)} - W_{aa}^{(2,-1)}\right] \neq 0$$

and

$$\left[W_{ab}^{(2,-1)} + W_{ba}^{(2,-1)}\right] \neq 0;$$

it is also easy to verify that

$$\left[\Gamma_{bbc}^{(3,-1)} - \Gamma_{aac}^{(3,-1)}\right] \neq 0$$

and

$$\left[\Gamma_{abc}^{(3,-1)} + \Gamma_{bac}^{(3,-1)}\right] \neq 0.$$

As in the case of Cr_2O_3, there are several indications suggesting that orbital magnetism should also exist in V_2O_3. We would like to draw the attention to the experimental fact that the parallel magnetic susceptibility does not drop to zero at low temperatures for V_2O_3 and Cr_2O_3 [104, 105]. This was again interpreted as the signature of a temperature-independent Van Vleck orbital magnetism. Very recently, Tanaka developed an interesting model [106] according to which each vanadium ion with $S = 1$ also has an orbital magnetic moment approximately given by $0.7\mu_B$; it was even suggested in [106] that these orbital moments can be slightly tilted away from the plane of the antiferromagnetic spin lattice, with the practical consequence that the $2/m \otimes \Theta$ symmetry is broken, thus making the low-temperature phase magnetoelectric. This would be consistent with the observation of a nonreciprocal XMLD spectrum if we additionally admit that there is locally some ordered electric dipole. Precisely this was recently considered in [27], where it was suggested that some cooperative Jahn–Teller distortion occurring at the monoclinic phase transition would also tilt the electric moments. We note that the development of an antiferroelectric order is compatible with the magnetoelectric group $2/m'$ and can possibly explain the highly destructive character of the phase transition for single crystals of any size. Indeed, as discussed in the previous subsection, there is still the risk that due to the core hole perturbation, the cross terms in Eq. (3) allow probing some pseudoground state of artificially reduced symmetry because core hole perturbation mixes the true ground state with low crystal field levels.

Recently, Di Matteo and Jansen [107] reported that they failed to measure any magnetoelectric susceptibility using the same single crystal as the one used in our nonreciprocal XMLD experiment, and they immediately questioned our interpretation. They also doubted the efficiency of the annealing process in our experiment by alleging that the conductivity of the $(V_{1-x}Cr_x)_2O_3$ crystal would exceed the conductivity losses of Cr_2O_3 by 15 orders of magnitude. According to our own tests, this figure is erroneously excessive. At the Néel temperature T_N, the conductivity of the $(V_{1-x}Cr_x)_2O_3$ crystal (approximately $3 \cdot 10^3\ \Omega \cdot$ cm [108]) was estimated to be 5 orders of magnitude higher than the measured conductivity (0.3 $G\Omega \cdot$ cm) of our Cr_2O_3 crystal. Under such conditions, the calculated dielectric relaxation time $\tau_R \approx 0.36$ ms (to be compared with $\tau_R \approx 36$ s for Cr_2O_3) still looks compatible with the fast microscopic dynamics of the magnetoelectric annealing process, as long as one accepts a low leakage current ($< 10\mu$A)) at the polarizing electrodes in order to evacuate the accumulated charges[1)]. It seems to us that the static magnetic field method apparently used in [107] to measure the magnetoelectric susceptibility of this chromium-doped vanadium sesquioxide crystal is totally inappropriate for systems that have rather large conductivity losses as explained in classical textbooks on magnetoelectric media [51]; this is precisely why pulse methods or methods exploiting magnetic fields modulated at a very high frequency were developed by several groups in the late sixties, in particular by Al'shin and Astrov, who used an alternating magnetic field at the frequency 4 MHz. Thus, due to the conductivity losses of the crystal, the failure of the experiments reported in [107] is not unexpected, but the inadequacy of the experimental

[1)] F. de Bergevin drew our attention to this important point. This led us to check the reality of a low leakage current which we had neglected in our reports.

method does not allow them to draw any conclusion regarding the questioned magnetoelectric nature of this $(V_{1-x}Cr_x)_2O_3$ crystal in the low-temperature monoclinic phase.

Anyhow, comparison of XOA experiments with magnetoelectric susceptibility measurements is not straightforward, as is illustrated by the following differences.

1) Nonreciprocal XOA probes only the orbital part of some average, spinless, one-electron magnetoelectric tensor. In contrast, macroscopic magnetoelectric susceptibility measurements have been discussed up to now essentially by considering in the first place how the spins are supposed to be ordered in a given low-temperature phase. Nothing is really known, however, regarding the relative contributions of the spin and orbital currents in such a magnetoelectric solid and it is not even clear whether magnetoelectric susceptibility measurements would be sensitive enough to detect a contribution of orbital currents. One can easily imagine a situation where some terms of the magnetoelectric tensor have a purely orbital origin or a vanishingly small spin contribution: in this case, the standard magnetoelectric susceptibility measurement can possibly fail and lead to erroneous conclusions. One may also envisage the converse case of magnetoelectric solids where the orbital part of the magnetoelectric tensor is partially quenched: there might exist geometries under which no XOA can be detected, even though the standard magnetoelectric susceptibility measurements allow expecting a signal.

2) Nonreciprocal XOA yields a local, element-selective information that cannot be obtained by conventional magnetoelectric susceptibility measurements. This could be turned into a formidable advantage if several absorption edges can be probed selectively. This advantage has a counterpart, however, the perturbation induced by the deep core hole might jeopardize the possibility to draw firm conclusions regarding the magnetic symmetry of the true ground state as a consequence of Eq. (3).

3) Macroscopic magnetoelectric susceptibility measurements require the use of intense electric or magnetic fields. In contrast, nonreciprocal XOA experiments *per se* do not require any electric/magnetic field and are inherently insensible to the conductivity losses of the sample. In the experiment discussed in this section, a magnetoelectric annealing process was used only to create remanent magnetoelectric states of opposite time-reversality. Other types of annealing could possibly produce the same result, for example, galvanomagnetic annealing or simply magnetic annealing could suffice under proper symmetry conditions. Figure 1 is a typical example where the action of the magnetic field on a spin anapole induces a local electric polarization and can induce the nucleation of an antiferroelectric order, without applying any electric field. The existence of an orbital anapole could possibly play the same role.

4.2. Effective operators and cross densities of states

4.2.1. Applications of the XOA sum rules

In this subsection, we wish to report on the first attempts that we made to use Carra–Jerez–Marri Eqs. (7)–(9) in order to derive the expectation values of the relevant $E1E2$ effective operators. It is instructive to first compare some practical details concerning the XOA sum rules and the XMCD sum rules in the soft X-ray range [24, 110].

1) Renormalizing the XOA dichroism spectra against the XANES spectra cannot exempt us from calculating the two radial integrals $R_\ell^{(1,2)}$ numerically. We found that this can be most conveniently done with the so-called FDMNES code [111], because we could easily check that these integrals are nearly constant over the energy range selected for the integration.

2) The XOA sum rules do not introduce any renormalization with respect to the number of holes in the band accepting the photoelectron, as this is typically the case with the XMCD sum rules.

3) In establishing the sum rules, we implicitly considered transitions between atomic multiplets of pure configurations, with ℓ_c, ℓ, and ℓ' being well identified quantum numbers. This may restrict Eqs. (7)–(9) to $E1E2$ transitions towards partially filled, localized bands of the finite width

$$\Delta E = E_{cutoff} - E_{Fermi}.$$

There is some ambiguity regarding the definition of E_{cutoff}, however. It is rather unclear whether one should set the cutoff energy at the inflexion point of the edge spectrum or beyond the most intense signatures of the dichroism spectra, i.e., slightly above the absorption edge. In order to warrant the numerical stability of the calculations, we were led to systematically set E_{cutoff} above the edge, but this is rather questionable when strong shape resonances of chiral-EXAFS signatures contribute to the experimental spectra.

4) In our opinion, the most serious difficulty is still of experimental nature and concerns the extreme sensitivity of the sum rules to baseline distortions that may be caused by instabilities of the X-ray beam or

by radiation damages to the sample. These problems can hardly be avoided over long data acquisition times. Error bars therefore strongly depend on the amplitude of the measured dichroism.

In Table 7, we have regrouped the expectation values of the effective operators that were extracted from our nonreciprocal XOA experiments using Eqs. (8) and (9). Two calculations were carried out systematically. In the first one, we assumed that the contribution of the septor $\mathbf{\Gamma}_{0,\pm2}^{(3,-1)}$ can be neglected; in the second, we assumed that the whole dichroism is entirely due to this septor term. As discussed in the previous sections, the second assumption is highly improbable regarding the measured XMχD spectra of Cr_2O_3; this is why the corresponding result is only quoted in parentheses. For the nonreciprocal XMLD experiments, the situation is more ambiguous due to the lack of information regarding the exact orientation of the crystal. Under the present conditions, the only option is to refer to the laboratory frame, and therefore the relevant effective operator is to be written as $\left[W_{XY}^{(2,-1)} + W_{YX}^{(2,-1)}\right]$. By analogy with the previous case, one may guess that the contribution of the septor terms must be negligible.

It appears clearly from Table 7 that the expectation value of the anapole moment is rather small for Cr_2O_3. Because we missed any pertinent reference for comparison, we tried to convert the calculated orbital anapole moment into an average toroidal dipole moment per unit cell using the relation

$$\mathbf{M}_{td}^{orb} = \frac{N\left\langle \mathbf{\Omega}_0 \right\rangle}{6} = 0.02\mu_B a_0,$$

where N is here the number of Cr atoms per unit cell and a_0 is the Bohr radius. It then becomes immediately obvious that $\mathbf{M}_{td}^{orb}$ is several orders of magnitude smaller than the spin toroidal dipole moment

$$\mathbf{M}_{td}^{spin} = 45\mu_B a_0$$

that was reported recently for the magnetoelectric crystal $Ga_{2-x}Fe_xO_3$ [109]. If this comparison makes sense, it would leave virtually no hope to extract the orbital part of the magnetoelectric tensor $[a_{\alpha\beta}]_{orb}$ from magnetoelectric susceptibility measurements, because such measurements are not sufficiently accurate at present. Interestingly, the values quoted for $\left[\left\langle W_{XY}^{(2,-1)}\right\rangle + \left\langle W_{YX}^{(2,-1)}\right\rangle\right]$ in the antiferromagnetic insulating phase of the $(V_{1-x}Cr_x)_2O_3$ crystal are one order of magnitude larger. As expected, the sign is reversed for magnetoelectric domains of opposite time-reversality. We recall that in our nonreciprocal XMLD experiments, we essentially measure a linear combination of $\left[W_{bb}^{(2,-1)} - W_{aa}^{(2,-1)}\right]$ and $\left[W_{ab}^{(2,-1)} + W_{ba}^{(2,-1)}\right]$, whereas in XM$\chi$D experiments, one would measure $\left[W_{ab}^{(2,-1)} - W_{ba}^{(2,-1)}\right]$. Thus, the preliminary result quoted in Table 7 for

$$\left[\left\langle W_{XY}^{(2,-1)}\right\rangle + \left\langle W_{YX}^{(2,-1)}\right\rangle\right] \approx \pm 0.8 \text{ a.u.}$$

looks rather consistent with the model proposed in [106], where a rather large ground state orbital moment is predicted for V_2O_3, while this is certainly not true for Cr_2O_3.

To illustrate the case of the XNCD sum rules, we have selected the cobalt K-edge XNCD spectra of the two enantiomeric complexes

$$\mathbf{1}^{(\pm)} = 2[\mathrm{Co(en)_3Cl_3}] \cdot \mathrm{NaCl} \cdot 6\mathrm{H_2O}$$

(see [18]), which were introduced in Sec. 3.2.1. In Table 8, we have also included additional results taken from our XNCD spectra data base:

1) the titanium K-edge XNCD spectra of two nonenantiomorphous crystals of potassium titanyl phosphate, i.e., $\mathbf{3} = \mathrm{KTiOPO_4}$ (space group $Pna2_1$, class $mm2$); these crystals were cut normal to the conjugated directions [120] and $[1\bar{2}0]$;

2) the iodine L_1-edge XNCD spectrum of lithium iodate, i.e., $\mathbf{4} = \mathrm{LiIO_3}$ (space group $P6_3$, class 6);

3) the tellurium L_1-edge XNCD spectrum of paratellurite, i.e., $\mathbf{5} = \mathrm{TeO_2}$ (space group $P4_12_12$, class 422).

As confirmed by Table 8, the pseudodeviators

$$\left\langle \mathbf{N}^{(2,+1)}\right\rangle = \left\langle [\mathbf{L}, \mathbf{\Omega}]^{(2)}\right\rangle$$

of the enantiomers $\mathbf{1}^{(+)}$ and $\mathbf{1}^{(-)}$ have nearly the same absolute value but opposite signs as anticipated from symmetry. In fact, the complex $\mathbf{1}^{(\pm)}$ turned to be the most favorable example due to its very strong pre-edge XNCD signal. For the potassium titanyl phosphate crystals, one would expect $\left\langle \mathbf{N}^{(2,+1)}\right\rangle$ to exhibit inverted signs in the case of XNCD spectra recorded with the wave vector parallel to the directions [120] and $[1\bar{2}0]$. In practice, the situation is much less favorable because there are two inequivalent Ti sites in the unit cell and we found them to contribute to dichroisms of the opposite signs [112]. The XNCD signal measured at the Ti K-edge is therefore very weak and the poor signal-to-noise ratio makes it more difficult to exploit the sum rule quantitatively. Nevertheless, the calculated values of $\left\langle \mathbf{N}^{(2,+1)}\right\rangle$ have the expected opposite signs and their low magnitudes are consistent with the average of the effective operator over the two inequivalent Ti sites.

Table 7. Expectation values of the nonreciprocal XOA operators

Compound	Cr K-edge Cr_2O_3		V K-edge V_2O_3 [H^+]		V K-edge V_2O_3 [H^-]	
Effective operator atom. units	Ω_z 0.03	$\Gamma_z^{(3)}$ (-0.03)	$W_{XY}^{(2)}+W_{YX}^{(2)}$ -0.84	$\Gamma_{YYZ}^{(3)}-\Gamma_{XXZ}^{(3)}$ (-0.48)	$W_{XY}^{(2)}+W_{YX}^{(2)}$ $+0.90$	$\Gamma_{YYZ}^{(3)}-\Gamma_{XXZ}^{(3)}$ $(+0.52)$
$R^{(1)}$ rad. integral	$-8.21\cdot10^{-5}$	$-8.21\cdot10^{-5}$	$-9.47\cdot10^{-5}$	$-9.47\cdot10^{-5}$	$-9.47\cdot10^{-5}$	$-9.47\cdot10^{-5}$
$R^{(2)}$ rad. integral	$-7.62\cdot10^{-6}$	$-7.62\cdot10^{-6}$	$-1.03\cdot10^{-5}$	$-1.03\cdot10^{-5}$	$-1.03\cdot10^{-5}$	$-1.03\cdot10^{-5}$

Table 8. Expectation values of the XNCD operators

Compound Absorption edge	$Coen_3[+]$ Co K-edge	$Coen_3[-]$ Co K-edge	$KTiOPO_4$ [120] Ti K-edge	$KTiOPO_4$ [$1\bar{2}0$] Ti K-edge	$LiIO_3$ I L_1-edge	TeO_2 Te L_1-edge
Effective operator atom. units	$\langle[\mathbf{L},\boldsymbol{\Omega}]^{(2)}\rangle$ $+0.424$	$\langle[\mathbf{L},\boldsymbol{\Omega}]^{(2)}\rangle$ -0.409	$\langle[\mathbf{L},\boldsymbol{\Omega}]^{(2)}\rangle$ $+0.016$	$\langle[\mathbf{L},\boldsymbol{\Omega}]^{(2)}\rangle$ -0.011	$\langle[\mathbf{L},\boldsymbol{\Omega}]^{(2)}\rangle$ $+0.50$	$\langle[\mathbf{L},\boldsymbol{\Omega}]^{(2)}\rangle$ $+0.77$
$R^{(1)}$ rad. integral	$-5.31\cdot10^{-5}$	$-5.31\cdot10^{-5}$	$-1.15\cdot10^{-4}$	$-1.15\cdot10^{-4}$	$2.33\cdot10^{-5}$	$2.53\cdot10^{-5}$
$R^{(2)}$ rad. integral	$-3.96\cdot10^{-6}$	$-3.96\cdot10^{-6}$	$-1.27\cdot10^{-5}$	$-1.27\cdot10^{-5}$	$-2.16\cdot10^{-6}$	$-2.57\cdot10^{-6}$

4.2.2. Cross densities of states

The requirement that the final states are localized is a severe restriction, especially in the so-called «chiral-EXAFS» regime which we have explored in the case of TeO_2 [19]. One may thus question whether Eq. (7) is suitable to analyze the iodine L_1-edge XNCD spectrum of α-$LiIO_3$, because in this particular example, the most intense signatures are clearly located in the continuum [16], i.e., well beyond the intense $2s \to 5p$ white line. In the continuum of states, we are convinced that it may be a better strategy in the context of XOA to transpose the so-called «differential» formulation of the sum rule, which is now commonly used to analyze the K-edge X-ray magnetic circular dichroism (XMCD) spectra in the so-called «Magnetic-EXAFS» regime [113–115]. Such a «differential» reformulation of Eq. (2) is given by

$$\frac{\Delta\sigma(E)}{E^2} \approx \frac{4\pi^2\alpha}{\hbar c}\sqrt{\frac{2\pi}{45}}\frac{S_3}{S_0}\times \times\frac{d}{dE}\left\{\sum_\beta Y_2^{\beta *} R_\ell^{(1)} R_{\ell'}^{(2)}\gamma(\ell,\ell')\times \times\left\langle\psi_f\left|\mathbf{N}_\beta^{(2,+1)}(\ell,\ell')\right|\psi_f\right\rangle\right\}, \quad (17)$$

where $\mathbf{N}^{(2,+1)}$ can be identified with $[\mathbf{L},\boldsymbol{\Omega}]^{(2)}$ and $\gamma(\ell,\ell')$ is a numerical factor. In this monoelectronic approach, we can define cross densities of states (X-DOS) $\langle\mathbf{N}^{(2,+1)}(E)\rangle$ that are related to the retarded one-electron Green's function $G^+(E)$ by

$$\left\langle\mathbf{N}^{(2,+1)}(E)\right\rangle = = -\frac{1}{\pi}\mathrm{Tr}\left\{\mathbf{N}^{(2,+1)}(\ell,\ell')\,\mathrm{Im}\,G^+(E)\right\}. \quad (18)$$

It follows from this definition that these cross densities of states refer to the effective operator of XNCD, i.e.,

$$\mathbf{N}^{(2)} = [\mathbf{L},\boldsymbol{\Omega}]^{(2)}.$$

According to Eq. (17), experimentally measured XNCD spectra must be directly proportional to the X-DOSs. This is confirmed by Fig. 8, where experimental and simulated iodine L_1-edge XNCD spectra of α-$LiIO_3$ are compared with the $(p-d)$ X-DOS calculated with a LMTO code [116]. The agreement looks very encouraging and clearly stimulates us to try extending Eqs. (17), (18) to nonreciprocal optical activity.

We finally note that although the definition of cross densities of states makes no reference to the ground state properties (Ψ_g), this does not mean that the deep core hole has no influence on their calculation.

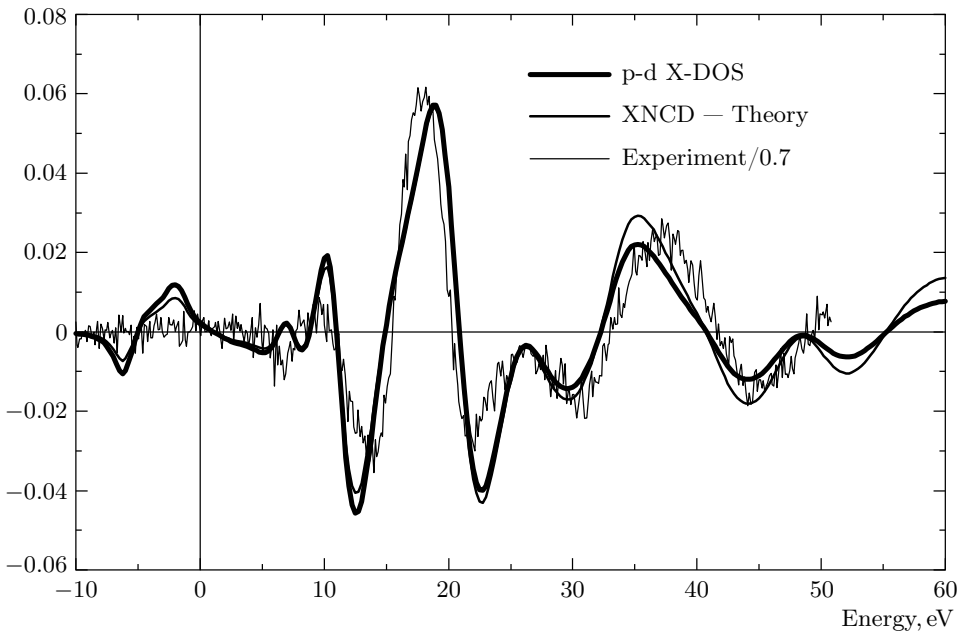

Fig. 8. Comparison of the experimental iodine L_1-XNCD spectrum of $LiIO_3$ with the calculated p–d cross density of states and the simulated XNCD spectrum

5. CONCLUSION

In conclusion, X-ray optical activity appears as a new, element-specific spectroscopy to study orbital magnetism in parity nonconserving solids. As far as the proposed $E1E2$ sum rules may give us access to the true ground state expectation values of magnetoelectric orbital operators, the nonreciprocal XOA might reveal hidden space–time symmetry properties in magnetoelectric crystals, because XOA probes only the weak orbital part of a monoelectronic magnetoelectric tensor, whereas it is extremely difficult to disentangle the orbital part from the spin part in classical magnetoelectric susceptibility measurements. For instance, XOA can reveal a reduction of the magnetic symmetry whenever the partially unquenched angular momentum has a quantization axis different from the one of the spins. We note, however, that the $E1E2$ sum rules can yield the expectation values of the pertinent parity-mixing operators only for a pseudo ground state. Due to the strong perturbation caused by the deep core hole, we cannot exclude a contribution of cross terms involving the ground state and low-lying excited states, as is the case with the temperature-independent Van Vleck paramagnetism. In this context, we note that a contribution of the Van Vleck paramagnetism to XMCD has been observed very recently at the same ESRF beamline in a paramagnetic insulator (EuF_3) and a paramagnetic metal (Pd) [117].

In this paper, we have clarified which time-reversal odd effective operator should be responsible for the magnetochiral dichroism XMχD (S_0) and the nonreciprocal linear dichroisms XMLD (S_1, S_2). The comparison of the nonreciprocal dichroism spectra recorded with single crystals or powdered samples has been shown to be particularly helpful in evaluating the relative importance of the higher-order septor $\langle \mathbf{\Gamma}^{(3,-1)} \rangle$ terms with respect to the contributions of the orbital anapole $\langle \mathbf{\Omega}^{(1,-1)} \rangle$ or the pseudodeviator $\langle \mathbf{W}^{(2,-1)} \rangle$. In the specific case of Cr_2O_3, there is very little doubt left that the observed magnetochiral dichroism is related to the orbital anapole operator. On the other hand, the orbital toroidal moment ($\mathbf{M}_{td}$) derived from the sum rule was found to be several orders of magnitude smaller than the spin $\mathbf{M}_{td}$ that was determined independently for a typical magnetoelectric crystal from diffraction data; this result seems to confirm that it would be very difficult to access to the orbital part of the magnetoelectric tensor using conventional magnetoelectric susceptibility measurements.

Potential applications of natural XOA in inorganic or bio-inorganic chemistry are still heavily impeded by the prerequisite that one should first obtain large-size single crystals of the resolved enantiomers in order to be able to record accurate XNCD spectra. We have shown that this difficulty can be circumvented if, for

instance, the chiral species is soluble in a liquid crystal phase that can be aligned in a magnetic field. We are still seeking further alternative approaches. The time-even pseudodeviator

$$\left\langle \mathbf{N}^{(2,+1)} \right\rangle = \left\langle [\mathbf{L}, \mathbf{\Omega}]^{(2)} \right\rangle$$

could be used to study and quantify ligand-induced asymmetry effects that are suspected to play an important role in asymmetric synthesis. More work is underway in order to extend the calculation of cross density of states and make their systematic numerical simulations possible.

The authors are particularly indebted to E. Katz for drawing their attention to the formulation of the orbital anapole given in [2] and for many stimulating discussions. They wish to thank C. Moise and D. Perey (Laboratoire de Synthèse & Electrosynthèse Organométalliques, Université de Bourgogne, Dijon) who carried out the synthesis and purification of the chiral compound **2**. One of us (Ch. B.) is grateful to S. Di Matteo and C. R. Natoli for communicating a preprint before publication. This work was supported in part by the INTAS (grant № 01-822) and IPGP (grant № 1921).

APPENDIX

The $E1E2$ absorption cross section was given in Eq. (4) as a product of spherical tensors $\mathbf{T}_\beta^{(b,\theta)}$ describing the X-rays and $\sigma_\beta^{(b,\theta)}$ describing the sample. Here, we give the relation between the sample spherical tensors $\sigma_\beta^{(b,\theta)}$ and the sample Cartesian tensor

$$A_{lmn} + iA'_{lmn} = \\ = 4\pi^2 \alpha \hbar \omega k i \sum_f \langle \psi_g | r_l | \psi_f \rangle \langle \psi_f | r_m r_n | \psi_g \rangle \times \\ \times \delta(E_f - E_g - \hbar\omega), \quad \text{(A.1)}$$

where A_{lmn} and A'_{lmn} are real. With this relation, the tables given in [49] can be used to determine the form of the sample spherical tensors as a function of the magnetic point group. From the definition of the sample Cartesian tensor, it is clear that $A_{lmn} = A_{lnm}$. This property must therefore be added when using the tables in [49]. The sample Cartesian tensor is parity-odd. To investigate its transformation under time-reversal symmetry, we replace $|\psi_f\rangle$ and $|\psi_g\rangle$ with $|\Theta\psi_f\rangle$ and $|\Theta\psi_g\rangle$ in Eq. (A.1), which gives

$$\Theta(A_{lmn} + iA'_{lmn}) = -(A_{lmn} + iA'_{lmn})^*.$$

Therefore, A_{lmn} is time-reversal odd and A'_{lmn} is time-reversal even. The relation between spherical and Cartesian tensors is given by the following formulas:

$$\sigma_{\pm1}^{(1,-1)} = \pm\frac{1}{\sqrt{30}}(2A_{xxx} \pm 3iA_{xxy} - A_{xyy} - \\ - A_{xzz} \mp iA_{yxx} + 3A_{xyy} \pm 2iA_{yyy} \mp iA_{yzz} + \\ + 3A_{zxz} \pm 3iA_{zyz}), \quad \text{(A.2)}$$
$$\sigma_0^{(1,-1)} = -\frac{1}{\sqrt{15}}(3A_{xxz} + 3A_{yyz} - A_{zxx} - \\ - A_{zyy} + 2A_{zzz});$$

$$\sigma_{\pm2}^{(2,-1)} = \mp\frac{1}{\sqrt{6}}(A_{xxz} \pm iA_{xyz} \pm iA_{yxz} - \\ - A_{yyz} - A_{zxx} \mp 2iA_{zxy} + A_{zyy}), \\ \sigma_{\pm1}^{(2,-1)} = \frac{1}{\sqrt{6}}(\pm iA_{xxy} - A_{xyy} + A_{xzz} \mp \quad \text{(A.3)} \\ \mp iA_{yxx} + A_{yxy} \pm iA_{yzz} - A_{zxz} \mp iA_{zyz}), \\ \sigma_0^{(2,-1)} = i(A_{yxz} - A_{xyz});$$

$$\sigma_{\pm3}^{(3,-1)} = \mp\frac{1}{2\sqrt{2}}(A_{xxx} \pm 2iA_{xxy} - A_{xyy} \pm \\ \pm iA_{yxx} - 2A_{yxy} \mp iA_{yyy}), \\ \sigma_{\pm2}^{(3,-1)} = \frac{1}{2\sqrt{3}}(2A_{xxz} \pm 2iA_{xyz} \pm 2iA_{yxz} - \\ - 2A_{yyz} + A_{zxx} \pm 2iA_{zxy} - A_{zyy}), \\ \sigma_{\pm1}^{(3,-1)} = \pm\frac{1}{2\sqrt{30}}(3A_{xxx} \pm 2iA_{xxy} + A_{xyy} - \quad \text{(A.4)} \\ -4A_{xzz} \pm iA_{yxx} + 2A_{yxy} \pm 3iA_{yyy} \mp 4iA_{yzz} - \\ - 8A_{zxz} \mp 8iA_{zyz}), \\ \sigma_0^{(3,-1)} = -\frac{1}{\sqrt{10}}(2A_{xxz} + 2A_{yyz} + A_{zxx} + \\ + A_{zyy} - 2A_{zzz}).$$

Finally,

$$\sigma_{\pm2}^{(2,+1)} = \frac{1}{\sqrt{6}}(\mp iA'_{xxz} + A'_{xyz} + A'_{yxz} \pm \\ \pm iA'_{yyz} \pm iA'_{zxx} - 2A'_{zxy} \mp iA'_{zyy}), \\ \sigma_{\pm1}^{(2,+1)} = \mp\frac{1}{\sqrt{6}}(A'_{xxy} \pm iA'_{xyy} \mp iA'_{xzz} - \quad \text{(A.5)} \\ - A'_{yxx} \mp iA'_{yxy} + A'_{yzz} \pm iA'_{zxz} - A'_{zyz}), \\ \sigma_0^{(2,+1)} = A'_{xyz} - A'_{yxz}.$$

REFERENCES

1. Ya. B. Zel'dovich, Sov. Phys. JETP **6**, 1184 (1958).

2. I. B. Khriplovich, *Parity Non-conservation in Atomic Phenomena*, Gordon and Breach Science Publ., New York (1991).

3. M-A. Bouchiat and C. Bouchiat, Rep. Prog. Phys. **60**, 1351 (1997).

4. C. S. Wood, S. C. Bennett, D. Cho, B. P. Masterson, J. L. Roberts, C. E. Tanner, and C. E. Wieman, Science **275**, 1759 (1997).

5. V. M. Dubovik and A. A. Cheskov, Sov. J. Particles Nucl. **5**, 318 (1975).

6. V. M. Dubovik, S. S. Krotov, and V. V. Tugushev, Sov. Phys. Crystallogr. **32**, 314 (1988).

7. V. M. Dubovik and V. V. Tugushev, Phys. Rep. **187**, 145 (1990).

8. V. L. Ginsburg, A. A. Gorbatsevitch, Yu. V. Kopaev, and B. A. Volkov, Sol. St. Comm. **50**, 339 (1984).

9. I. E. Dzyaloshinskii, Sov. Phys. JETP **10**, 628 (1960).

10. J. Goulon, C. Goulon-Ginet, A. Rogalev, V. Gotte, Ch. Brouder, and C. Malgrange, Eur. Phys. J. B **12**, 373 (1999).

11. A. D. Buckingham, Adv. Chem. Phys. **12**, 107 (1968).

12. L. D. Barron, *Molecular Light Scattering and Optical Activity*, Cambridge University Press, Cambridge (1982).

13. J. W. Cooper, Phys. Rev. A **47**, 1841 (1993).

14. J. Goulon, A. Rogalev, F. Wilhelm, C. Goulon-Ginet, P. Carra, D. Cabaret, and Ch. Brouder, Phys. Rev. Lett. **88**, 237401-1 (2002).

15. J. Goulon, C. Goulon-Ginet, A. Rogalev, G. Benayoun, Ch. Brouder, C. Malgrange, and P. A. Metcalf, Phys. Rev. Lett. **85**, 4385 (2000).

16. J. Goulon, C. Goulon-Ginet, A. Rogalev, V. Gotte, C. Malgrange, Ch. Brouder, and C. R. Natoli, J. Chem. Phys. **108**, 6394 (1998).

17. L. Alagna, T. Prosperi, S. Turchini, J. Goulon, A. Rogalev, C. Goulon-Ginet, C. R. Natoli, R. D. Peacock, and B. Stewart, Phys. Rev. Lett. **80**, 4799 (1998).

18. B. Stewart, R. D. Peacock, L. Alagna, T. Prosperi, S. Turchini, J. Goulon, A. Rogalev, and C. Goulon-Ginet, J. Am. Chem. Soc. **121**, 10233 (1999).

19. J. Goulon, C. Goulon-Ginet, A. Rogalev, G. Benayoun, Ch. Brouder, and C. R. Natoli, J. Synchrotron Rad. **7**, 182 (2000).

20. C. R. Natoli, Ch. Brouder, Ph. Sainctavit, J. Goulon, C. Goulon-Ginet, and A. Rogalev, Eur. Phys. J. B **4**, 1 (1998).

21. J. A. Schouten, *Tensor Analysis for Physicists*, Clarendon Press, Oxford (1964).

22. J. Jerphagnon, D. Chemla, and R. Bonneville, Adv. Phys. **27**, 609 (1978).

23. A. J. Starace, Phys. Rev. B **5**, 1773 (1972).

24. B. T. Thole, P. Carra, F. Sette, and G. van der Laan, Phys. Rev. Lett. **68**, 1943 (1992).

25. S. Di Matteo and C. R. Natoli, J. Synchrotron Rad. **9**, 9 (2002).

26. D. A. Varshalovich, A. N. Moskalev, and V. K. Khersonskii, *Quantum Theory of Angular Momentum*, Word Scientific Publishing Co. Pte Ltd, New York (1988).

27. P. Carra, A. Jerez, and I. Marri, E-print archives, cond-mat/0104582.

28. J. Luo, G. T. Trammell, and J. P. Hannon, Phys. Rev. Lett. **71**, 287 (1993).

29. W. Ludwig and C. Falter, *Symmetries in Physics*, Springer Verlag, Berlin (1988).

30. E. P. Wigner, *Group Theory*, Academic Press, New York (1960).

31. R. G. Sachs, *The Physics of Time Reversal*, University of Chicago Press, Chicago (1987).

32. Ch. Brouder, J. Phys.: Cond. Mat. **2**, 701 (1990).

33. L. C. Biedenharn and J. D. Louck *The Racah-Wigner Algebra in Quantum Theory*, Addison-Wesley, Reading (1981).

34. J. Tenenbaum, Proc. Indian Acad. Sci. A **64**, 74 (1967).

35. P. Carra and R. Benoist, Phys. Rev. B **62**, R7703 (2000).

36. P. Carra, J. Mag. Mag. Mat. **233**, 8 (2001).

37. P. Carra, A. Jerez, and I. Marri, Phys. Rev. B **67**, 045111 (2003).

38. S. Brasselet and J. Zyss, J. Opt. Soc. Am. B **15**, 257 (1998).

39. E. Ascher, Helvetica Phys. Acta **39,** 40 (1966).

40. E. E. Radescu and D. H. Vlad, Phys. Rev. E **57**, 6030 (1998).

41. A. A. Gorbatsevich, Yu. V. Kopaev, and V. V. Tugushev, Sov. Phys. JETP **58**, 643 (1983).

42. A. A. Gorbatsevich and Y. Kopaev, Ferroelectrics **161** 321 (1994).

43. R. R. Lewis, Phys. Rev. A **49**, 3376 (1994).

44. L. D. Landau and E. M. Lifshitz, *Statistical Physics*, MIR Editions, Moscow (1951).

45. K. Siratori, K. Kohn, and E. Kita, Acta Physica Polonica A **81**, 431 (1992).

46. P. Carra, H. König, B. T. Thole, and M. Altarelli, Physica B **192**, 182 (1993).

47. G. van der Laan, Phys. Rev. B **57**, 112 (1998).

48. G. van der Laan, B. T. Thole, G. A. Sawatzky, J. B. Goedkoop, J. C. Fuggle, J. M. Esteva, R. Karnatak, J. P. Remeika, and H. A. Dabkowska, Phys. Rev. B **34**, 6529 (1986).

49. R. R. Birss, *Symmetry and Magnetism*, *Series on Selected Topics in Solid State Physics*, ed. by E. P. Wohlfarth, North-Holland Publishing Company, Amsterdam (1964), Vol. III.

50. J.-P. Rivera, Ferroelectrics **161**, 165 (1994).

51. T. H. O'Dell, *The Electrodynamics of Magneto-Electric Media*, *Series on Selected Topics in Solid State Physics*, ed. by E. P. Wohlfarth, North-Holland Publishing Company, Amsterdam (1970), Vol. XI.

52. E. Ascher, Phil. Mag. **17**, 149 (1968).

53. N. B. Baranova and B. Ya Zel'dovich, Mol. Phys. **38**, 1085 (1979).

54. G. Wagnière and A. Meier, Chem. Phys. Lett. **93**, 78 (1982).

55. L. D. Barron and J. Vrbancich, Mol. Phys. **51**, 715 (1984).

56. G. L. J. A. Rikken and E. Raupach, Nature **390**, 493 (1997).

57. G. L. J. A. Rikken, E. Raupach, V. Krstic, and S. Roth, Mol. Phys. **100**, 1155 (2002).

58. P. Kleindienst and G. H. Wagnière, Chem. Phys. Lett. **288**, 89 (1998).

59. N. G. Kalugin, P. Kleindienst, and G. H. Wagnière, Chem. Phys. **248**, 105 (1999).

60. S. L. Hou and N. Bloembergen, Phys. Rev. A **138**, 1218 (1965).

61. V. A. Avetisov and V. I. Gol'danskii, Physics-Uspekhi **39**, 819 (1996).

62. J. L. Bada, Nature **374**, 594 (1995).

63. S. F. Mason and G. E. Tranter, Proc. Royal. Soc. (London) A **397**, 45 (1985).

64. L. Pasteur, *Revue Scientifique* **VII**, 2 (1884).

65. W. Voigt, Ann. Phys. (Leipzig) **18**, 651 (1905).

66. F. I. Fedorov, Opt. Spectrosc. (USSR) **6**, 237 (1959).

67. J. Jerphagnon and D. Chemla, J. Chem. Phys. **65**, 1522 (1976).

68. E. B. Graham and R. E. Raab, Philos. Mag. **66**, 269 (1992).

69. J. Goulon, A. Rogalev et al., private communication.

70. J. Goulon, A. Rogalev, C. Train, M. Verdaguer et al., private communication.

71. H. Brünner and J. Doppelberger, Bull. Soc. Chim. Belge **84**, 923 (1975).

72. A. Saupe and G. Englert, Phys. Rev. Lett. **11**, 462 (1963).

73. H. Kelker and R. Hatz, *Handbook of Liquid Crystals*, Verlag Chemie, Weinheim-Basel (1980).

74. D. N. Astrov, Sov. Phys. JETP **13**, 729 (1961).

75. B. I. Al'shin and D. N. Astrov, Sov. Phys. JETP **17**, 809 (1963).

76. T. H. O'Dell, Phil. Mag. **13**, 921 (1966)

77. S. Shtrikman and D. Treves, Phys. Rev. **130**, 986 (1963).

78. R. M. Hornreich, in *Magnetoelectric Interaction Phenomema in Crystals*, ed. by A. J. Freeman and H. Schmid, Gordon and Breach, London (1975), p. 211.

79. J. Goulon et al., private communication.

80. S. Foner and M. Hanabusa, J. Appl. Phys. **34**, 1246 (1963).

81. J. Ohtani and S. Kohn, J. Phys. Soc. Jpn. **53**, 3744 (1984).

82. D. V. Belov, G. P. Vorob'ev, A. M. Kadomtseva, Yu. Popov, and A. K. Zvezdin, JETP Lett. **58**, 581 (1993).

83. Yu. Popov, A. M. Kadomtseva, D. V. Belov, G. P. Vorob'ev, and A. K. Zvezdin, JETP Lett. **69**, 330 (1999).

84. S. S. Krotov, A. M. Kadomtseva, Yu. F. Popov, A. K. Zvezdin, G. P. Vorob'ev, and D. V. Belov, J. Magn. and Magn. Mat. **226–230**, 963 (2001).

85. M. Fiebig, D. Fröhlich, and H.-J. Thiele, Phys. Rev. B **54**, R12 681 (1996).

86. V. P. Plakthy, Sol. St. Comm. **79**, 313 (1991).

87. S. Foner, Phys. Rev. **130**, 183 (1963).

88. S. D. Silverstein and I. S. Jacobs, Phys. Rev. Lett. **12**, 670 (1964).

89. W. H. Brumage, C. R. Quade, and C. C. Lin, Phys. Rev. **131**, 949 (1963).

90. M. Muto, Y. Tanabe, T. Izuka-Sakano, and E. Hanamura, Phys. Rev. B **57**, 9586 (1998).

91. L. M. Corliss, J. M. Hastings, R. Nathans, and G. Shirane J. Appl. Phys. **36**, 1099 (1965).

92. E. J. Samuelsen, M. T. Hutchings, and G. Shirane, Physica **48**, 13 (1970).

93. P. J. Brown, J. B. Forsyth, E. Lelièvre-Berna, and F. Tasset, J. Phys.: Cond. Mat. **14**, 1957 (2002).

94. M. Catti, G. Sandrone, G. Valerio, and R. Dovesi, J. Phys. Chem. Solids **57**, 1735 (1996).

95. M. Catti, G. Sandrone, and R. Dovesi, Phys. Rev. B **55**, 16122 (1997).

96. R. Kubo and Y. Obata, J. Phys. Soc. Jpn. **11**, 547 (1956).

97. S. Greenwald, Nature **177**, 286 (1956).

98. R. E. Word, S. A. Werner, W. B. Yelon, J. M. Honig, and S. Shivashankar, Phys. Rev. B **23**, 3533 (1981).

99. W. B. Yelon, S. E. Werner, and R. E. Word, J. Appl. Phys. **52**, 2237 (1980).

100. R. M. Moon, Phys. Rev. Lett. **25**, 527 (1970).

101. M. Yethiraj, J. Sol. St. Chem. **88**, 53 (1990).

102. S. Di Matteo, N. B. Perkins, and C. R. Natoli, Phys. Rev. B **65**, 054413 (2002).

103. L. Paolasini, C. Vettier, F. de Bergevin, A. Sollier, W. Neubeck, F. Yakhou, P. A. Metcalf, and J. M. Honig, Phys. Rev. Lett. **82**, 4719 (1999).

104. P. H. Carr and S. Foner, J. Appl. Phys. **31**, 344S (1960).

105. M. Greenwood, R. W. Mires, and A. R. Smith, J. Chem. Phys. Lett. **54**, 1417 (1971).

106. A. Tanaka, J. Phys. Soc. Jpn. **71**, 1091 (2002).

107. S. Di Matteo and A. G. M. Jansen, Phys. Rev. B **66**, 100402R (2002).

108. H. Kuwamoto, J. M. Honig, and J. Appel, Phys. Rev. B **22**, 2626 (1980).

109. Yu. Popov, A. M. Kadomtseva, G. P. Vorob'ev, V. A. Timofeeva, D. M. Ustinin, A. K. Zvezdin, and M. M. Tegeranchi, JETP **87**, 146 (1998).

110. R. Wu, D. Wang, and A. J. Freeman, Phys. Rev. Lett. **71**, 3581 (1993).

111. Y. Joly, Phys. Rev. B **63**, 125120 (2001).

112. G. Benayoun, Ph. D. Thesis, Université Joseph Fourier, Grenoble (2001).

113. P. Strange, H. Ebert, J. B. Staunton, and B. L. Gyorffy, J. Phys.: Cond. Mat. **1**, 2959 (1989).

114. H. Ebert, Rep. Prog. Phys. **59**, 1665 (1996).

115. G.Y. Guo, J. Phys.: Cond. Mat. **8**, L-747 (1996).

116. O. K. Andersen and O. Jepsen, Phys. Rev. Lett. **53**, 2571 (1984).

117. A. Rogalev, F. Wilhelm et al., submitted to J. Magn. Magn. Mat.